CIRA(EXT)004
February 1996

NATIONAL PHYSICAL LABORATORY

MCNP Calculation of Neutron Scatter in the Main Bay of the Chadwick Building, NPL

O F Naismith and D J Thomas
Centre for Ionizing Radiation & Acoustics

© Crown copyright 1996
Reproduced by permission of the Controller of HMSO

ISSN 1361-4053

National Physical Laboratory
Teddington, Middlesex, UK, TW11 0LW

Extracts from this report may be reproduced
provided the source is acknowledged

Approved on behalf of Managing Director NPL, by Dr Peter Christmas
Director, Centre for Ionizing Radiation and Acoustics.

SUMMARY

The Monte Carlo neutron transport code MCNP has been used to calculate the room and air scattered neutron component at 75 cm from a radionuclide source located at the centre of the low-scatter area in the Chadwick Building, Bldg. 47, at NPL. This is the standard distance used for calibrating personal dosemeters, and the calculation provides information for correcting the response of dosemeters to the scattered radiation. Calculations were performed for both an Am-Be and a ^{252}Cf source. The results were checked by measurements with a Bonner sphere spectrometer set. These measurements revealed that the model used for features within the low-scatter area needs to be refined for calculating scatter at distances further from the source than 75 cm.

CONTENTS

1. INTRODUCTION

The usual procedure for the calibration of neutron instruments employs a source of neutrons of known emission rate, traceable to national standards, to irradiate an instrument whose response is then related to the neutron fluence or dose equivalent to obtain a calibration factor. The calibration factor should be a unique property of the device and the neutron source spectrum, and should not be a function of the characteristics of the calibration facility. When neutron instruments are calibrated, they respond to neutrons scattered in the air and walls of the room as well as to the source neutrons. A calibration measurement must be corrected to the reading which would be obtained for the 'uncontaminated' neutron field direct from the source, i.e. with no contribution from neutron scatter. This is termed the "free-field response".

Neutron scatter is the largest source of uncertainty in the fluence delivered during an irradiation. Incident neutrons from the source may be scattered out of the path of the detector by air molecules between the source and detector, or can be scattered into the detector by air or structural material present in the irradiation room, such as the walls of the room or the detector stand. Each of these contributions needs to be accounted for in some way in order to derive the correct calibration factor for the device.

The error introduced by neutron scatter to the calibration factor for a device cannot be simply accounted for by the difference in the neutron fluence. The scattering process affects not only the total fluence but also the spectrum of neutrons arriving at the detector. Since the response of an instrument varies with neutron energy the effect of the scatter is dependent on both the energy spectrum of the scattered neutrons and the energy-response function of the device; different corrections will, in general, be necessary for different detector response functions. Scattered neutrons necessarily have a lower energy than the incident neutron. Since devices used for neutron radiation protection monitoring are designed to have a response which matches that of the dose equivalent curve, which rises rapidly above 50 keV, the effect of neutron scatter on dosemeter response is likely to be less than the difference in fluence. In fact, since some personal dosemeters have an energy threshold of a few hundred keV, neutron scatter may have very little effect on the calibration of these devices.

Neutron irradiations at the National Physical Laboratory are carried out in the low-scatter facility in Building 47, Chadwick Building. This is a large room, of approximate dimensions 17 m x 23 m and height 18 m. The large size of the room is important in minimising room-scatter. Although the walls are thick concrete in order to shield the surrounding environment from radiation, the roof is relatively thin. The floor has been removed from an area 6 m in radius around the source position, which is near the centre of the room, and a few low-density 'walkways' have been installed to allow access. However, these walkways and other material present near the source or detector, such as support stands and the arms on which the detector stands are located, will act as additional sources of neutron scatter.

Two radionuclide neutron sources are used for routine calibrations: ^{241}Am-Be(α,n) and ^{252}Cf spontaneous fission sources encapsulated in stainless steel. Both sources provide spectra with a fast neutron distribution, which peak at about 4 MeV and 2 MeV respectively. ^{252}Cf sources generally have a higher neutron emission rate and can be used for calibrations where a large neutron fluence rate is required.

2. TECHNIQUES FOR DETERMINING NEUTRON SCATTER

Measurements of neutron scatter, and in particular the individual components contributing to the total scatter effect, are difficult to perform. However, scattering is amenable to calculation. Modern Monte Carlo transport codes provide a simple and efficient means of estimating neutron scatter for a particular source, room configuration, and position within that room. Another approach is to predict the scatter contribution by analytical techniques, using a generalised model of the calibration room(1). However, this approach has not been discussed here.

There are several experimental techniques that can be used to evaluate scattering corrections, whose applicability depends on the type of instrument to be calibrated and the size and shape of the calibration room. These methods can be grouped into two categories. The first involves measurement of the scattered neutron component itself by means of a neutron-absorbent 'shadow cone' placed between the source and detector. The second involves measuring only the total response to all neutrons. A combination of calculations and measurements at a range of distances is then used to correct the observed response to the response from source neutrons alone.

The most common, and intuitively obvious, experimental approach to correct for neutron scatter is the shadow cone technique. The shadow cones used at NPL consist of two parts, a 20 cm long iron front end and a 30 cm long rear section made of boron-loaded polyethylene or paraffin wax. This combination has negligible transmission for neutrons emitted by the recommended radioactive neutron sources. Each cone has a different half-angle so that an appropriate one can be chosen for any reasonable source-detector distance and detector size. With a cone in place, the detector is exposed only to in-scattered neutrons, from the air, the surfaces of the calibration room, and any other material in the room. The detector response to scattered neutrons can then be subtracted from the full response, with no shadow cone present, to obtain the response to neutrons coming directly from the source.

In the semi-empirical method and the polynomial fit method a fit is obtained to a set of data measured at a series of distances from the source, from which the free-field response can be derived. With the semi-empirical method, the response to the room-scatter component can be estimated from the gradient and intercept of the plot. The coefficients of the polynomial fit have no direct physical relevance, but this technique is more widely applicable and has fewer physical limitations. A more extensive discussion of these techniques can be found in reference 2. Note that both of these methods rely upon a stable instrument response which is linear throughout the measurement dose and dose rate range.

One limitation of the experimental techniques is that they are practical only for active instrumentation, such as area survey meters, where consecutive measurements can be made with the same device. In the case of personal dosemeters, which are passive devices (although electronic neutron personal dosemeters are currently under development), the effect of neutron scatter is usually minimised by using the smallest practical source-to-detector distance. (ISO recommend a calibration distance of 75 cm(3)). Allowance is then made in the uncertainty on the neutron fluence to cover the small but unknown scatter component.

The data provided by such measurements are only applicable to the instrument irradiated, and in the case of the shadow cone technique to the particular measurement position within the irradiation room. To obtain data applicable to a wide range of instruments the spectral fluence would be required.

The only spectrometer capable of measurement across the whole spectrum, from below thermal energy up to several MeV, is a Bonner sphere set. The experiment necessitates a series of measurements using different-sized spheres, which must be repeated with a shadow cone located between the source and detector. However, because the scatter contribution is likely to be small compared to the direct fast neutron component the uncertainties on the scatter spectrum are likely to be high. The measurements and subsequent unfolding of the data are time-consuming, and the results relate only to a single measurement position.

3. NEUTRON SCATTER

Proper calibration procedures require that the instrument reading be corrected for the effects of neutrons scattered by the neutron source support, the air between the source and instrument (in-scatter and out-scatter), and the walls of the calibration room. Typically, the correction for source support is small - of the order of 1%. Air scattering also amounts to a few percent in general. However, since the albedo of fast neutrons from concrete and other building materials is greater than 0.5[4], the contribution of room-reflected neutrons to the response of the dosemeter may be significant, particularly if the dosemeter is sensitive to the low energy neutrons resulting from room-scatter.

Studies[1] have shown that the response of an instrument to neutrons scattered from the surface of a spherical cavity is constant everywhere and therefore not dependent on the distance from the source. This relationship breaks down in the case of a typical calibration room, where the distance to the floor or ceiling is less than that to the walls, and the floor and ceiling become the main sources of reflected neutrons. However, for isotropic sources at or near the centre of a calibration room the room-return component remains approximately constant in a region near the source, where most calibrations are performed.

In small and moderate-sized calibration rooms (linear dimensions $\leq$10 m) the effect of room-scattered neutrons completely dominates air scattering. Even in much larger rooms, residual room scatter and scatter by instrument support stands may be comparable with air scatter. Air in-scattering is approximately twice the out-scattering, so the net effect is always to increase the fluence at the detector. Calculations[5] have shown that the relative fluence due to air scatter increases linearly with distance over the range covered in a typical calibration (up to 5 m). Since single scattering dominates the air-scattered neutron spectrum for distances up to a few metres, the air-scattered spectrum does not vary with distance over this range. This spectrum is, however, different from that of the source neutrons, as is the angular distribution. The effect of air scattered neutrons on dosemeter response is discussed in reference 5.

4. MCNP CALCULATION

MCNP is a general-purpose Monte Carlo neutron transport code developed at the Los Alamos National Laboratory in the USA[6]. In addition to neutron and photon transport, version 4A covers electron interactions. The code can be obtained from the NEA Data Bank in France, and is extensively used by laboratories and industry worldwide. MCNP is ideally suited to calculate neutron scatter in calibration rooms, and was thus chosen to calculate the scatter spectrum in the main calibration hall of the Chadwick Building at NPL.

The user creates an input file that is subsequently read by MCNP. This file specifies information about the problem such as the geometry, materials, evaluated cross-sections, location and characteristics of the neutron source, the quantities to be tallied, and any variance reduction techniques to be used to improve the efficiency of the calculation.

The nuclear data libraries cover the energy range 10^{-5} eV to 20 MeV, and most of the important reactions are included in any particular evaluation. Continuous-energy neutron interaction data for each element were extracted from three libraries: ENDF/B version IV or earlier, the Lawrence Livermore National Laboratory's Evaluated Nuclear Data Library, ENDL, and the Los Alamos Sub-library, LASL-SUB. The most recent evaluation available was selected for each element.

Structures are modelled within MCNP using the intersection and union of surfaces (planes, spheres, cylinders, tori, cones, etc.) to enclose a volume and then specifying a material for the geometric cell defined in this way.

The dimensions of the Main Bay were extracted from the technical drawings drawn up at the time of the refurbishment of Building 47. This gave the height and thickness of the walls, floor, and ceiling of the irradiation room and those immediately adjacent, e.g. the accelerator room, the labyrinth and the basement. It was also used to locate the position and approximate size of other features in the room such as the pit circle and the thermal pile. The model was subsequently simplified to remove those regions or features which made an insignificant contribution to the scatter at the measurement position.

The walls of each room were generally about 1 m thick. The Main Bay incorporates a labyrinth leading to the control room, which follows through to the Van de Graaff accelerator room. Since there is no solid concrete floor under the irradiation area some details of the basement rooms underneath were included in the model. Finally, towards the east, the hall extends into the source cell area from where high emission rate sources can be transported automatically into their irradiation position. The roof of the low-scatter facility is relatively thin, consisting of a 15 cm concrete layer topped by aluminium pleating. The aluminium was neglected in the model, since its neutron-reflective properties were assumed to be insignificant compared with the inner concrete layer.

The dimensions of features such as the thermal pile were determined either by direct measurement or from existing reports describing the facilities. The thermal pile is located to the north-east of the room, between the pit-circle and source cell, and is essentially a graphite moderator in the form of a rectangular block 279 cm long by 144 cm wide by 156 cm high, shielded with an 18 cm layer of paraffin wax contained in wooden boxes(7). Every effort was made to include structures in the immediate vicinity of the source or detector since they could constitute a significant source of neutron in-scatter.

The 'pit-circle' is a region 6 m in radius about the source position at the centre of the low- scatter facility. Access to the middle is by one of three "cheese segment" walkways, made from lightweight Aerolam® board. The board contains a core of aluminium honeycomb, of nominal density 83 kg m^{-3}, sandwiched between 0.55 mm thick aluminium alloy skins. There are four tubular arms in the pit-circle which can be rotated about the source position. However, only three were included in the model since the definition of cylinders in MCNP is restricted to the direction of the co-ordinate axes. These were arranged one along the x-axis and two along the y-axis, one on either side of the centre of the pit-circle. The tubes are made from an aluminium alloy, H30, with a density of 2.7 g cm^{-3}, and are 22.9 cm in diameter and 1.27 cm thick. A detector carriage is attached to each arm which allows automatic movement of the detector with reference to the source position. The rod which holds the radionuclide source at the centre of the pit-circle has been modelled because of its proximity to the neutron source and hence its potential for neutron scatter. The 'floor' outside the pit circle is a steel grid, which has been modelled as a metal sheet with the same thickness as the floor but with density adjusted to account for the volume of metal in each grid element.

Plots of various two-dimensional sections through the MCNP model can be seen in Figures 1 to 7. These illustrate the large-scale structure of the Main Bay and some of the finer detail included in the model, for example the pit-circle.

The material compositions, densities, and cross-section evaluations used in the calculation are tabulated in Appendix 1. The composition of concrete was unknown, in particular the proportion of iron. It was therefore estimated, and an additional calculation performed with a higher proportion of iron to establish the effect on room-scatter. Calculations were performed both with and without air to provide an estimate of the effect of air scatter. The cross-sections were primarily from the ENDF/B-IV and ENDL85 libraries. Some older data were used where more recent evaluations were not available.

Two different source spectra were used for the calculations, ^{241}Am-Be and ^{252}Cf, which are the two radionuclide sources most commonly used for calibrations. The ^{241}Am-Be group fluence spectrum was entered as a histogram distribution on an MCNP source card, using the ISO-recommended spectrum(8). MCNP has some built-in analytic functions which can be used to generate a continuous probability density function for the source variable. The Maxwell fission spectrum, whose probability function is

$$p(E) = C\, E^{1/2} \exp(-E/a)$$

was used to approximate the ^{252}Cf energy spectrum. The parameter "a" is the temperature of the distribution (1.42 MeV for ^{252}Cf), and this parameter and the function number (-2) were input on a source bias card.

The source spectra are defined as the spectra generated by the active material; most calibration sources are lightly encapsulated so that the scattering is small and the resulting spectrum change is negligible. An isotropic point source was specified, ignoring the inherent anisotropy of a cylindrical source, and was positioned at the centre of the pit-circle 1 m above the 'floor'.

The MCNP tally cards specify what type of information the user wants to derive from the Monte Carlo calculation; e.g. current across a surface, flux at a point, heating in a region, etc. Two types of tally were used to determine the spectral fluence. The first was the F4 tally, fluence averaged over a cell, in which any neutrons entering the defined volume are recorded. This is therefore the most 'realistic' method of tallying the fluence at any position. A spherical shell 1 cm thick and 20 cm high, with its front surface at the appropriate calibration distance, was defined around the source position as the tallying cell, to represent the field at the phantom position averaged over 360° around the source plane. However, this technique is very inefficient considering the small solid angle subtended by the source to the tally cell, and the small volume of this cell compared to the total volume of the room.

The other tally used was the ring detector, F5, which provides a deterministic estimate of the fluence at a point in space, sampled from some location on a ring defined about a coordinate axis, and is made at source and collision events throughout the random walk. The fluctuation on the data should be lower than that of the F4 tally because of the larger number of events contributing. Both types of tally were used for the calculations in order to provide some validation of the results.

The recommended distance of a dosemeter from the neutron source for the calibration of personal dosemeters is 75 cm[(3)], chosen to minimise the effect of room-return while keeping the uncertainty in the distance and the variation in fluence across the surface of the phantom to an acceptable level. This was therefore the distance used for the calculations: both as the radius of the ring detector about the source position and of the inner sphere of the F4 tally cell. In addition data were tallied at 150 cm from the source in order to validate the results against experiment, since measurements using the shadow cone technique are not possible so close to the source.

The spectrum of the scattered field was tallied according to a logarithmic energy bin structure, with five bins per energy decade. The output gives the number of neutrons in each energy bin per source neutron together with an uncertainty estimate. In the case of the ring detector two sets of data are produced: the total spectrum (direct plus scatter) and the 'uncollided' spectrum direct from the source. The total fluence per source neutron is also calculated.

In addition to the scatter spectra, tallies were made of the neutron leakage from the roof of the low-scatter facility and through the wall adjacent to the Control Room, using the F4 tally with a thin volume covering the relevant area defined as the tally cell.

The MCNP input file for the ^{252}Cf calculation is given in Appendix 2. In order to obtain acceptable statistics on the results (reducing the uncertainties on the F5 tally spectrum to within 4% for each energy bin) 5 x 10^5 histories were tallied for each run. The program, version 4A, was run on a 486DX 66 MHz personal computer, which took roughly 20 hours to perform each calculation.

5. RESULTS

The results of all four calculations are presented in Table 1 below, which gives the total neutron fluence for the F4 and F5 tallies at two distances from the source. The ring detector tally is accompanied by some diagnostics to test the validity of the results (variance reduction techniques are very susceptible to errors if misused) and a list of the contribution to the scattered fluence of each cell defined in the problem. This is very useful in determining the most significant sources of neutron scatter. The F4 tally fluence is derived from the ratio of the average tally per history to the tally cell volume.

For each tally fluctuation charts are tabulated which show the variation in the tally, uncertainty and figure of merit as the number of particles run increases. These provide an indication of the reliability of the data.

Table 1. Total neutron fluence at 75 cm and 150 cm from two neutron sources (units cm^{-2}).

	^{252}Cf		^{241}Am-Be	
	Air	Vacuum	Air	Vacuum
75 cm				
F4 cell tally	1.482×10^{-5}	1.478×10^{-5}	1.467×10^{-5}	1.456×10^{-5}
Ring detector (total)	1.488×10^{-5}	1.479×10^{-5}	1.478×10^{-5}	1.471×10^{-5}
" " (uncollided)	1.403×10^{-5}	1.415×10^{-5}	1.405×10^{-5}	1.415×10^{-5}
150 cm				
F4 cell tally	4.141×10^{-6}	4.079×10^{-6}	4.002×10^{-6}	3.970×10^{-6}
Ring detector (total)	4.116×10^{-6}	4.090×10^{-6}	4.030×10^{-6}	4.012×10^{-6}
" " (uncollided)	3.479×10^{-6}	3.537×10^{-6}	3.488×10^{-6}	3.537×10^{-6}

The errors on the F4 cell tallies were 0.4% at 75 cm and 0.6% at 150 cm. Those on the ring detector (F5) tallies were less: 0.04% at 75 cm and 0.05% at 150 cm. The 'uncollided' neutron flux was assumed to have no uncertainty.

The ring detector spectra tallied for each source (for the calculations including air) are given in Appendix 3. The data have been plotted in Figures 8 and 9 for both the F4 and F5 tallies, together with the uncollided (direct) source spectrum at each distance. The figures show that there is good agreement between the two tally types, and hence the ring detector can be assumed to provide a reliable estimate of the spectrum. The main difference is due to the fluctuation in the F4 results in the intermediate energy region where the fluence is low and hence where there are large uncertainties associated with the data (of 50% or more). The error estimates on the ring detector tally are much lower and thus the spectrum appears smoother.

The direct 'free-field' fluence at a distance *d* from an isotropic source can be calculated using the inverse square law as $1/4\pi d^2$ per source neutron, which yields a fluence of 1.415×10^{-5} cm^{-2} at 75 cm and 3.537×10^{-6} cm^{-2} at 150 cm. These values agree with the F5 'uncollided' tally for the calculations in vacuum. Since this tally estimates the contribution of neutrons reaching the detector that have not undergone any interactions, the difference between the air and vacuum results must be the air out-scatter. Air out-scatter can also be calculated using the expression:

$1 - \exp(-\Sigma_a d)$

as a fraction of the free-field fluence, where Σ_a is the spectrum-averaged macroscopic neutron total cross-section of air and d the distance from the source. The values of Σ_a, calculated by folding both the oxygen and nitrogen cross-sections over the neutron source spectrum, are 1060 x 10^{-7} cm^{-1} for ^{252}Cf and 880 x 10^{-7} cm^{-1} for ^{241}Am-Be[(2)]. The MCNP calculations are compared with the predicted air out-scatter in Table 2. The two sets of data are in good agreement providing an additional validation of the MCNP calculation.

Table 2. Air out-scatter calculated using MCNP and analytically.

	^{252}Cf		^{241}Am-Be	
Distance from source	MCNP	Analytical	MCNP	Analytical
75 cm	-0.82%	-0.80%	-0.69%	-0.66%
150 cm	-1.62%	-1.60%	-1.37%	-1.33%

Neutron in-scatter can therefore be calculated by subtracting the uncollided fluence from the total fluence, and the results are presented in Table 3 as a percentage of the free-field fluence.

Table 3. Neutron in-scatter at two distances from the neutron source.

	^{252}Cf	^{241}Am-Be
In-scatter at 75 cm	6.0%	5.1%
In-scatter at 150 cm	18.0%	15.3%

The net scatter effect (in-scatter minus out-scatter) is the difference between the total fluence and the free-field fluence calculated using the inverse square law. The results are presented in Table 4 as the increase in the absolute fluence and as a ratio to the free-field fluence.

Table 4. Net increase in fluence from neutron scatter for ^{252}Cf and ^{241}Am-Be.

	^{252}Cf	^{241}Am-Be
Scatter at 75 cm (cm^{-2})	7.339 x 10^{-7} ± 0.6%	6.301 x 10^{-7} ± 1.0%
" as ratio to free-field fluence	5.2%	4.5%
Scatter at 150 cm (cm^{-2})	5.789 x 10^{-7} ± 0.4%	4.934 x 10^{-7} ± 0.4%
" as ratio to free-field fluence	16.4%	13.9%

Although the free-field fluence falls according to the inverse square law, the thermal fluence of the scatter spectrum (see Figures 8 and 9) seems to be independent of the distance from the source;

similarly for the intermediate energy region. At 150 cm the absolute value of the scattered fluence was only 15% to 20% lower than that at 75 cm. This resulted in a much larger scatter contribution relative to the free-field fluence: 16% and 14% for ^{252}Cf and ^{241}Am-Be respectively, compared with only 5% at 75 cm.

The sum of the group fluence (per source neutron) up to 1 keV was very similar at both irradiation distances, which indicates that room-scatter (from which these lower energy neutrons are presumed to originate) is approximately constant throughout the central region of the irradiation room. However, calculations for a wider range of distances would be necessary in order to confirm this theory.

The in-scattered spectra for the calculations including air and those without are plotted in Figures 10 and 11, for ^{252}Cf and ^{241}Am-Be, at the two irradiation distances. The data were derived by subtracting the 'uncollided' spectrum from the total spectrum of the F5 tally.

The fluence in the thermal energy region increased by approximately 20% when air was removed from the calculation. The fast neutron fluence (above 50 keV) was much higher for the with-air calculations (by 70% at 75 cm and 50% at 150 cm), and the difference was more marked for the ^{252}Cf source than for ^{241}Am-Be.

The contribution due to room-return and air in-scatter cannot be separated by a simple comparison of calculations with and without air because of multiple interactions: room-scattered neutrons may be scattered into or out of the path of the detector by air molecules. However, an estimate of each component can be made using the "contributions by cell" table in the diagnostics of the F5 tally output. The cells were divided into three groups: walls, floor or ceiling of the room, air, and structures located near the source (e.g. source rod, walkways, etc.). The results are presented in Table 5.

The data support the hypothesis that room-return is approximately constant throughout the central region of the room. The net air scatter, relative to the free-field neutron fluence, does increase with distance from the source, but the scatter increases more rapidly with distance than would be expected from a linear relationship. However, the air in-scatter estimation has been enhanced by scatter from the walls of the room since many room-returned neutrons will be further scattered in air before they reach the detector. Estimates of the relative air scatter fluence for both ^{252}Cf and ^{241}Am-Be are given in reference 5.

Table 5. Room-return, air in-scatter, and scatter due to structures near the source at two irradiation distances. The figure in brackets is the ratio to the free-field fluence.

	^{252}Cf	^{241}Am-Be
<u>75 cm</u>		
Room-return	3.10×10^{-7} cm^{-2} (2.2%)	2.70×10^{-7} cm^{-2} (1.9%)
Air in-scatter	3.67×10^{-7} cm^{-2} (2.6%)	3.05×10^{-7} cm^{-2} (2.2%)
Structures near source	1.65×10^{-7} cm^{-2} (1.2%)	1.52×10^{-7} cm^{-2} (1.1%)
<u>150 cm</u>		
Room-return	3.12×10^{-7} cm^{-2} (8.8%)	2.73×10^{-7} cm^{-2} (7.7%)
Air in-scatter	2.44×10^{-7} cm^{-2} (6.9%)	1.98×10^{-7} cm^{-2} (5.6%)
Structures near source	8.03×10^{-8} cm^{-2} (2.3%)	7.08×10^{-8} cm^{-2} (2.0%)

The ring detector tally can also be used to determine which cells make the largest contribution to the neutron in-scatter. The majority of the scatter is by the walls, floor and ceiling of the low-scatter facility (particularly the concrete floor at the base which contributes 14%), the air in the low-scatter facility (30%), and structures close to the source, namely the detector carriage tubes and the steel rod holding the source (both about 10%). The values are similar at 150 cm, but the source rod, which is now further from the tallying region, contributes less.

Since the elemental composition of the concrete walls was unknown, an additional calculation was performed with the proportion of iron in concrete increased by a factor of five to investigate the effect on neutron scatter. Both material compositions are given in Appendix 1. The calculation was performed using a ^{252}Cf source spectrum. The results indicate a decrease in the net scatter of about 3% at 75 cm and 5% at 150 cm. However, this represents a correction of only 0.2% to the total fluence at 75 cm and therefore any minor inaccuracies in the material composition are unlikely to significantly affect the results.

6. BONNER SPHERE MEASUREMENTS

Measurements of the scattered spectrum of a ^{252}Cf source were performed in the Main Bay using the NPL ^{3}He Bonner sphere set(9). The ^{252}Cf source 4775 NC (originally 100 μg) was used for the irradiations. Two sets of measurements were taken, one using a shadow cone to measure the scattered fluence. In order to correctly shadow each detector (i.e. prevent all direct neutrons reaching the sphere without over-shadowing the detector) measurements could not be made as close as 75 cm to the source; instead the spheres were positioned at a distance of 150 cm.

Six Bonner spheres were used for the measurements: 3.5", 4", 5", 6", 8" and 10" in diameter. The measured and calculated data were compared using the unfolding code STAYS'L, which compares the Bonner sphere responses with an a priori spectrum. The total and in-scattered spectra for the ^{252}Cf calculations at 150 cm were used as a priori information for STAYS'L and compared with the direct and shadow-cone measurements respectively for all six spheres. A standard deviation of 1% was assigned to the measured responses. For the a priori spectrum a standard deviation of 50% was assigned to each group fluence and all group fluences were correlated by a component having a 50% standard deviation.

The results of the unfolding for the scattered spectrum are plotted in Figure 12, and the spectral data are given in Appendix 4. A comparison of the measurement and calculation indicates that the calculation underestimates the high energy scatter and possibly overestimates the thermal component. The calculated scatter is about 18% of the free-field fluence, compared with the measured value of 23%; i.e. the measured scatter is 27% higher than the calculation.

Although the disagreement is quite large when the scatter component is viewed in isolation, the agreement for the total spectrum (i.e. scatter plus free-field) is good to about 6%. Also, the sphere measurements were made in the plane of the waist of the source, where the anisotropy factor is 1.02, whereas the calculations were for an isotropic source. This brings the measurement and calculation closer by 2% for the total fluence.

The main disagreement concerns the fast scatter. This suggests that the MCNP model may be missing some scattering material close to the source. Therefore an additional MCNP calculation was performed, restricted to the central volume of the low-scatter facility, to investigate the additional contribution of structures present for the measurements, such as the shadow-cone and detector support stands, to the total scatter. A point detector at 150 cm from the source and located directly above the detector support stand was used in addition to the ring detector. This model can be seen in Figure 13.

The results showed an increase of 12% in the neutron scatter, representing a 2% increase in the total fluence. However, 80% of this increase could be attributed to the use of the point detector instead of the ring detector (the point detector was located at the position of maximum scatter above the detector support stand; the ring detector averages over all locations around the source). This, in addition to some simplifications in the model, may explain much of the difference between the measured and calculated results. However, in the case of personal dosemeter irradiation measurements are often made at all angles around the source (e.g. free-in-air irradiations on a ring) and the two support stands required for the Bonner sphere measurements would not be present. Therefore the MCNP results may provide a more accurate estimate of the scattered fluence for personal dosemeter calibration.

7. EFFECT OF NEUTRON SCATTER ON DOSEMETER RESPONSE

In order to determine the effect of neutron scatter on dosemeter calibration, the full spectrum must be folded with the dosemeter response function and compared with the dosemeter response to the free-field neutron fluence. The spectra were therefore folded with a variety of commonly-used personal dosemeter and area survey meter response functions, using the program package SPKTBIB[10] which was written at NPL and PTB (Germany) and includes a database of neutron spectra, dosemeter response functions and dosimetric quantities. The response functions of the personal dosemeters considered have been plotted in Figure 14. The results for all dosemeters are presented in Table 6, and the value quoted is the percentage increase in fluence response for a dosemeter irradiated at 75 cm compared to the free-field response.

The effect of scatter on the calibration of both personal dosemeters and area survey meters seems to be a fairly consistent increase in response of 2% to 3% for either source. This is roughly half the increase in fluence, and is due to the fact that scattered neutrons have a lower energy than source neutrons and dosemeter response generally decreases below the fast neutron energy region. Also, some personal dosemeters have an energy threshold in the region of a few hundred keV and will not respond to neutrons below this energy. The second NTA film dosemeter has the highest energy threshold and no thermal response, and hence this dosemeter showed the least increase in response. However, a series of measurements using the shadow-cone technique with the Harwell 0949 remmeter indicated an increase in response of some 6%. This would seem to confirm the results of the Bonner sphere measurements, which showed a larger scatter component, and may be due to additional scattering by the detector and shadow-cone support stands.

Table 6. Increase in dosemeter fluence response at 75 cm due to neutron scatter.

	^{252}Cf	^{241}Am-Be
<u>Personal dosemeters</u>:		
237-neptunium	2.0%	0.4%
PADC (with thermal radiator)	2.9%	4.1%
PADC (without radiator)	2.9%	4.1%
NTA film (with thermal response)	3.0%	1.8%
NTA film (no thermal response)	1.9%	0.9%
<u>Area survey instruments</u>:		
Harwell 0949	2.7%	3.0%
Anderson-Braun (NM2)	3.0%	2.3%
Studsvik	1.6%	2.3%

The data in Table 6 are calculated for a dosemeter with an isotropic angular response. All personal dosemeters have a response which varies considerably with the angle of incidence. Since the response tends to decrease with angle of incidence on the dosemeter, the figures in the table can be viewed as upper limits to the effects of scatter. Another complicating factor is that many personal dosemeter irradiations are carried out on-phantom rather than free-in-air, and the presence of the phantom will affect both the spectrum and the fluence of scattered neutrons. In addition, the phantom of course creates neutron back-scatter itself.

8. LEAKAGE FROM THE ROOF AND CONTROL ROOM WALL

Neutron leakage from the roof of the low-scatter facility and the wall adjacent to the Control Room was tallied in addition to the source scatter spectra. The fluence and the mean energy of the field (derived from the output table "neutron activity in each cell") were used to estimate the dose rate that might be experienced outside these areas for a 'typical' neutron source of nominal emission rate 10^7 s^{-1}. The fluence-to-dose equivalent conversion factors used were derived from the coefficients of Wagner et al[11]. The results are presented in Table 7 below.

Table 7. Neutron leakage through the Main Bay roof and Control Room wall for a source emission rate of 10^7 s^{-1}.

Source	Fluence (cm^{-2})	Mean energy	H*(10) ($pSv\ cm^{-2}$)	Dose rate
Roof:				
^{252}Cf	3.043×10^{-8}	640 keV	280	0.3 μSv h^{-1}
^{241}Am-Be	1.221×10^{-10}	1.4 MeV	360	0.4 μSv h^{-1}
Control Room:				
^{252}Cf	3.203×10^{-8}	120 keV	90	0.4 nSv h^{-1}
^{241}Am-Be	1.916×10^{-10}	300 keV	180	1.2 nSv h^{-1}

9. DISCUSSION

MCNP is a very powerful tool for calculating effects such as neutron scatter where measurements are not practical or are difficult to perform. In the present application, in addition to the spectral data, information was also derived on the relative size of the in- and out-scatter contributions to the total scatter and the features of the room which contributed the most to this scatter.

The net increase in fluence at 75 cm was about 5% for ^{252}Cf and 4.5% for ^{241}Am-Be. The scatter was dominated by room-returned neutrons, whose contribution was roughly constant throughout the central region of the low-scatter facility. The effect of air out-scatter was also calculated from the tally results and agreed well with predicted values. The contributions of air scatter and room-return to the in-scattered fluence could not be distinguished since many room-scattered neutrons interacted further with air before reaching the detector. Approximately 10% of the in-scatter was due to equipment located near the source and detector.

MCNP calculations of the spectral fluence at 150 cm from a source were lower than the Bonner sphere measurements, in particular at fast neutron energies. This could be due to a variety of factors: scattering material unaccounted for near the source or detector (e.g. support stands for the measurements); the increase in measured fluence due to source anisotropy; or an under-estimate of air in-scatter, perhaps arising from air humidity. The difference in the net scatter was about 30%, but this represents a difference of only 6% between the absolute values of the total neutron fluence.

The effect of neutron scatter on the calibration of a personal dosemeter is an increase of up to 2% to 3% in the fluence response. Even this value is probably an over-estimate of the effect since the calculation assumes an isotopic angular response, and many calibrations are performed on-phantom which itself provides some shielding from room-scattered neutrons. However, the results presented here should help to provide a more accurate estimate of a scatter correction for personal dosemeter calibration than the present method of increasing the uncertainty estimate. The results were similar for area survey instruments, but measurements for these instruments are usually made at distances greater than one metre where neutron scatter can be accounted for by the shadow cone technique.

A useful extension of this work would be to calculate scatter spectra at a full range of distances, from which correction factors for a variety of instrumentation could be derived, eliminating the need for shadow cone measurements in routine calibrations. The results could also be used to further investigate some of the suggestions made in this report about the relationship between various scatter components and distance from the neutron source.

10. REFERENCES

C.M.Eisenhauer. *Review of Scattering Corrections for Calibration of Neutron Instruments*. Radiat. Prot. Dosim. **28**(4) pp.253-262 (1989).

2 C.M.Eisenhauer, J.B.Hunt and R.B.Schwartz. *Calibration Techniques for Neutron Personal Dosimetry*. Radiat. Prot. Dosim. **10**(1/4) pp.43-57 (1985).

3 International Organization for Standardization (ISO). *Procedures for Calibrating and Determining the Response of Neutron Measuring Devices used for Radiation Protection*. Draft Standard Proposal ISO/DIS 10647, ISO/TC 85/SC 2/WG 2/SG 3 (1993).

4 F.J.Allen, A.Futterer and W.Wright. *Dependence of Neutron Albedos upon Hydrogen Content of a Shield*. Ballistic Research Laboratories Report BRL-1224. Aberdeen, Maryland (1963).

5 C.M.Eisenhauer, R.B.Schwartz and R.C.McCall. *Effect of Air Scatter on Calibration of Instruments for Detecting Neutrons*. Radiat. Prot. Dosim. **19**(2) pp.77-84 (1987).

6 J.F.Briesmeister. *MCNP - A General Monte Carlo Code for Neutron and Photon Transport (Version 3A)*. LA-7396-M, Rev. 2 (September 1986).

T.B.Ryves and E.B.Paul. *The Construction and Calibration of a Standard Thermal Neutron Flux Facility at the NPL*. J. Nucl. Eng. **22** pp.759-775 (1968).

8 International Organization for Standardization (ISO). *Neutron Reference Radiations for Calibrating Neutron Measuring Devices used for Radiation Protection Purposes and for Determining their Response as a Function of Neutron Energy*. ISO 8529 (1989).

9 R.L.Bramblett, R.I.Ewing and T.W.Bonner. *New Type of Neutron Spectrometer*. Nucl. Instrum. Methods **9** pp.1-12 (1960).

10 O.F.Naismith and B.R.L.Siebert. *A Database of Neutron Spectra, Instrument Response Functions, and Dosimetric Conversion Factors for Radiation Protection Applications*. Radiat. Prot. Dosim. (to be published).

11 S.R.Wagner, B.Grosswendt, J.R.Harvey, A.J.Mill, H.-J.Selbach and B.R.L.Siebert. *Unified Conversion Functions for the New ICRU Operational Radiation Protection Quantities*. Radiat. Prot. Dosim. **12**(2) pp.231-235 (1985).

APPENDIX 1: Material Compositions

Material	MCNP Reference No.	Density (g cm^{-3})	Element	MCNP ZAID No.	Atom Fraction
Concrete	1	2.3	O Si H Al Ca Na Fe	8016.35 14000.35 1001.04 13027.35 20000.35 11023.35 26000.35	0.5454 0.2173 0.1798 0.0229 0.0173 0.0127 0.0046
Concrete (enhanced in iron)	1	2.4	O Si H Al Ca Na Fe	8016.35 14000.35 1001.04 13027.35 20000.35 11023.35 26000.35	0.5353 0.2133 0.1778 0.0225 0.0170 0.0125 0.0230
Air	2	0.00122	N O Ar C	7014.04 8016.35 18000.01 6012.35	0.7844 0.2107 0.0047 0.0002
Stainless steel (floor grid)	3	7.93 (1.0)	Fe Cr Ni Mn Si C	26000.35 24000.35 28000.11 25055.35 14000.35 6012.35	0.6935 0.1856 0.0934 0.0143 0.0121 0.0011
Graphite	4	2.25	C	6012.35	1.0
Paraffin wax	5	0.9	H C	1001.04 6012.35	0.6667 0.3333
Aluminium (walkway)	6	2.7 (0.083)	Al	13027.35	1.0

APPENDIX 2: MCNP Input File

```
NPL MAIN BAY SCATTER CALCULATION - 252-Cf including air: heavy concrete
c
c      Walls of room:
c
1      1  -2.3   1 -6 21 -35 41 -42  imp:n=1      $ base below low-scatter area
2      1  -2.3   1 -14 21 -35 51 -52  imp:n=1     $ roof above low-scatter area
3      1  -2.3   (1 -6 21 -22 42 -51):(6 -14 21 -22 43 -51)
       imp:n=1                                   $ x-z wall next to Control Room
4      1  -2.3   (1 -6 34 -35 42 -51):(6 -14 34 -35 43 -51)
       imp:n=1                                   $ x-z wall outside Main Bay
5      1  -2.3   1 -2  22 -34 42 -51  imp:n=1    $ back wall (y-z) of l-s area
8      2  -0.00122  2 -5 22 -34 42 -51 #(-23 -50) #22 #(33 -49) #51 #52
       #(23 -33 15 -16) #46 #47  imp:n=1         $ air in low-scatter facility
9      1  -2.3   13 -14 22 -34 49 -51  imp:n=1   $ y-z wall from roof to roof
                                                 $ above accelerator
10     1  -2.3   13 -14 22 -33 48 -49  imp:n=1   $ roof above accelerator
11     1  -2.3   5 -6 22 -34 42 -43  imp:n=1     $ y-z wall by base below low-
                                                 $ scatter area
12     1  -2.3   5 -14 22 -34 43 -44  imp:n=1    $ base below accelerator /
                                                 $ beam-lines
13     0   6 -14 21 -35 41 -43  imp:n=1          $ below accelerator region
15     1  -2.3   5 -14 23 -33 45 -46  imp:n=1    $ floor by beam-lines /
                                                 $ accelerator
16     2  -0.00122  5 -13 22 -34 48 -51 #(-50 -23) #(33 -49) #39
       imp:n=1                                   $ air above beamlines / roof
17     2  -0.00122  5 -10 23 -33 46 -48 #30 #35 #(-71 61 -62 63 -64)
       imp:n=1                                   $ air by beam-lines
18     2  -0.00122  5 -14 22 -33 44 -45 #27 #(-13 -23)  imp:n=1
                                                 $ air below beam-lines
20     1  -2.3   (22 -23 5 -13 44 -50):(22 -23 13 -14 45 -48)  imp:n=1
                                    $ " " between l-s and accelerator area
21     0  2 -3 22 -23 42 -50  imp:n=1  $ air btw. walls (x-z) by Control Room
22     1  -2.3  2 -4 23 -24 42 -50  imp:n=1      $ inner wall (x-z) by
                                                 $ Control Room
25     1  -2.3  2 -5 33 -34 42 -49  imp:n=1      $ inner wall (x-z) on outside
                                                 $ of low-scatter facility
26     1  -2.3  5 -14 33 -34 44 -49  imp:n=1     $ " " by outside of beamline /
                                                 $ source cell area
27     1  -2.3  13 -14 32 -33 44 -48 #15  imp:n=1  $ source cell wall (y-z)
29     1  -2.3  3 -5 22 -23 42 -50  imp:n=1      $ part of inner wall (x-z) by
                                                 $ Control Room
30     1  -2.3  9 -10 25 -27 46 -48  imp:n=1    $ rhs wall (x-z), accel-level,
                                                 $ forming part of entrance maze
32     1  -2.3  ((25 10 -11 55):(30 -31 -14 55):(55 -56 -30 11))
       (46 -48)  imp:n=1   $ wall (x-z) separating VdG and source cell areas
35     1  -2.3  7 -8 23 -26 46 -53  imp:n=1
                                    $ y-z wall forming part of entrance maze
37     0  10 -14 23 -33 46 -48 #27 #32  imp:n=1  $ air around accelerator
39     1  -2.3  48 -49 10 -13 23 -31 #(-31 10 -55)  imp:n=1
                                    $ front part of roof over accelerator room
c
c      Pit-circle and thermal pile
c
40     2  -0.00122  (2 -5 23 -33 15 -16) #(-4 -24) #48 #41 #42 #43 #44
       #45  imp:n=1                     $ air around pit-circle
41     6 -2.7   -60 84 -83  imp:n=1     $ detector carriage tube
42     6 -2.7   -60 -88 82 -80  imp:n=1  $ detector carriage tube
43     6 -0.083   -60 -90 87 93 -46  imp:n=1     $ walkway
44     6 -0.083   -60 91 92 87 93 -46  imp:n=1   $ walkway
45     6 -0.083   -60 -88 -89 -91 93 -46  imp:n=1  $ walkway (beam-lines)
46     3 -7.93   94 -95 17 -97  imp:n=1  $ lower source rod
47     3 -7.93   -96 97 -98  imp:n=1     $ upper source rod
48     3  -1.0  2 -5 54 -46 23 -33 60 #(-24 -4)  imp:n=1   $ steel grid floor
49     5  -0.9  46 -71 61 -62 63 -64 #50  imp:n=1  $ thermal pile - wax
50     4  -2.25  46 -70 66 -67 68 -69  imp:n=1     $ thermal pile - graphite
c
c      Tally cells
```

```
c
51    2  -0.00122  85 -86 73 -74   imp:n=1    $ detection cell (75cm)
52    2  -0.00122  65 -72 73 -74   imp:n=1    $ detection cell (150cm)
53    0  1 -14 21 -35 52 -79  imp:n=1   $ tally cell: roof above 1-s area
54    0  1 -14 77 -21 46 -50  imp:n=1   $ tally cell: Control Room wall
55    0  1 -14 77 -21 41 -79 #(46 -50)  imp:n=1
c
60    0  #(1 -14 77 -35 41 -79)   imp:n=0     $ neutron cut-off

1     px  -810
2     px  -720
3     px  410
4     px  530
5     px  620
6     px  665
7     px  960
8     px  990
9     px  1100
10    px  1510
11    px  1630
13    px  1830
14    px  1890
15    pz  467
16    pz  490.5
17    pz  491
21    py  -1060
22    py  -1030
23    py  -920
24    py  -860
25    py  -810
26    py  -770
27    py  -720
30    py  0
31    py  120
32    py  460
33    py  830
34    py  895
35    py  925
41    pz  0
42    pz  50
43    pz  210
44    pz  270
45    pz  460
46    pz  490
48    pz  790
49    pz  880
50    pz  1310
51    pz  1859
52    pz  1874
53    pz  690
54    pz  487
55    p   1.85 -1 0 3028
56    p   1.79 -1 0 3183
60    sz  490 610
61    p   0.575 1 0 674.3
62    p   0.575 1 0 882.1
63    p   1.733 -1 0 1149
64    p   1.733 -1 0 1780
65    sz  590 150
66    p   0.575 1 0 695.1
67    p   0.575 1 0 861.3
68    p   1.733 -1 0 1185
69    p   1.733 -1 0 1744
70    pz  706
71    pz  724
72    sz  590 151
73    pz  580
74    pz  600
77    py  -1061
79    pz  1875
80    c/x 0 478.6 11.4
```

```
82     c/x 0 478.6 10.1
83     c/y 0 478.6 11.4
84     c/y 0 478.6 10.1
85     sz  590 75
86     sz  590 76
87     px  11.4
88     px  -11.4
89     py  -11.4
90     p   1 -0.36 0 0
91     p   0.36 -1 0 0
92     p   0.36 1 0 0
93     pz  485
94     cz  2.25
95     cz  2.5
96     cz  0.4
97     pz  578
98     pz  589

sc1    CALIFORNIUM-252 SOURCE (MAXWELL FISSION SPECTRUM)
sdef   erg=d1 x=0 y=0 z=590
sp1    -2 1.42
c
c
fc4    SPECTRUM AT 75cm AROUND SOURCE POSITION
f4:n   51
e0     7.943E-10 1.259E-09 1.995E-09 3.162E-09 5.012E-09 7.943E-09
       1.259E-08 1.995E-08 3.162E-08 5.012E-08 7.943E-08 1.259E-07
       1.995E-07 3.162E-07 5.012E-07 7.943E-07 1.259E-06 1.995E-06
       3.162E-06 5.012E-06 7.943E-06 1.259E-05 1.995E-05 3.162E-05
       5.012E-05 7.943E-05 1.259E-04 1.995E-04 3.162E-04 5.012E-04
       7.943E-04 1.259E-03 1.995E-03 3.162E-03 5.012E-03 7.943E-03
       1.259E-02 1.995E-02 3.162E-02 5.012E-02 7.943E-02 1.259E-01
       1.995E-01 3.162E-01 5.012E-01 7.943E-01 1.259E+00 1.995E+00
       3.162E+00 5.012E+00 7.943E+00 1.259E+01 1.995E+01 3.162E+01
c
fc14   SPECTRUM AT 150cm AROUND SOURCE POSITION
f14:n 52
c
fc5    RING DETECTOR AT 75cm AROUND SOURCE
f5z:n   590 75 0
c
fc15   RING DETECTOR AT 150cm AROUND SOURCE
f15z:n 590 150 0
c
fc24   LEAKAGE THROUGH CELL 53 (roof)
f24:n 53
e24    30
c
fc34   LEAKAGE THROUGH CELL 54 (Control Room wall)
f34:n 54
e34    30
c
c
m1     1001.04 0.1798 8016 0.5454 14000 0.2173 26000 0.0046
       11023 0.0127 13027 0.0229 20000 0.0173  $ CONCRETE
m2     7014 0.7844 8016 0.2107 18000 0.0047 6012 0.0002  $ AIR
m3     26000 0.6935 24000 0.1856 28000 0.0934 25055 0.0143
       14000 0.0121 6012 0.0011  $ STEEL
m4     6012 1  $ GRAPHITE
m5     1001.04 0.6667 6012 0.3333  $ WAX
m6     13027 1  $ ALUMINIUM
c
c
phys:n  31.62 31.62  $ MAX ENERGY - ANALOG CAPTURE
c
nps    500000
```

APPENDIX 3: ^{252}Cf and ^{241}Am-Be spectra at 75 cm from the source.

	^{252}Cf		^{241}Am-Be	
Energy (MeV)	Fluence (cm^{-2})	% error	Fluence (cm^{-2})	% error
7.943 x 10^{-10}	3.576 x 10^{-11}	27.9 %	3.434 x 10^{-11}	32.3 %
1.259 x 10^{-9}	4.281 x 10^{-11}	24.6 %	5.846 x 10^{-11}	22.2 %
1.995 x 10^{-9}	1.557 x 10^{-10}	13.1 %	1.671 x 10^{-10}	12.9 %
3.162 x 10^{-9}	3.925 x 10^{-10}	8.5 %	3.531 x 10^{-10}	10.9 %
5.012 x 10^{-9}	1.402 x 10^{-9}	12.5 %	9.737 x 10^{-10}	6.1 %
7.943 x 10^{-9}	2.905 x 10^{-9}	4.9 %	2.648 x 10^{-9}	10.4 %
1.259 x 10^{-8}	5.991 x 10^{-9}	2.4 %	5.338 x 10^{-9}	3.4 %
1.995 x 10^{-8}	1.248 x 10^{-8}	1.9 %	1.130 x 10^{-8}	5.8 %
3.162 x 10^{-8}	2.266 x 10^{-8}	1.5 %	2.005 x 10^{-8}	3.2 %
5.012 x 10^{-8}	3.427 x 10^{-8}	1.2 %	2.812 x 10^{-8}	1.5 %
7.943 x 10^{-8}	3.861 x 10^{-8}	1.8 %	3.239 x 10^{-8}	1.4 %
1.259 x 10^{-7}	2.708 x 10^{-8}	1.8 %	2.172 x 10^{-8}	1.5 %
1.995 x 10^{-7}	1.162 x 10^{-8}	1.8 %	9.743 x 10^{-9}	2.3 %
3.162 x 10^{-7}	4.884 x 10^{-9}	2.8 %	4.035 x 10^{-9}	3.7 %
5.012 x 10^{-7}	4.123 x 10^{-9}	3.4 %	3.431 x 10^{-9}	6.9 %
7.943 x 10^{-7}	4.084 x 10^{-9}	3.6 %	3.003 x 10^{-9}	3.5 %
1.259 x 10^{-6}	4.092 x 10^{-9}	4.8 %	3.244 x 10^{-9}	3.8 %
1.995 x 10^{-6}	4.228 x 10^{-9}	2.9 %	3.266 x 10^{-9}	3.7 %
3.162 x 10^{-6}	4.052 x 10^{-9}	3.6 %	3.129 x 10^{-9}	3.7 %
5.012 x 10^{-6}	4.095 x 10^{-9}	2.9 %	3.201 x 10^{-9}	3.5 %
7.943 x 10^{-6}	4.008 x 10^{-9}	3.3 %	3.591 x 10^{-9}	4.0 %
1.259 x 10^{-5}	4.144 x 10^{-9}	2.8 %	3.666 x 10^{-9}	4.2 %
1.995 x 10^{-5}	4.484 x 10^{-9}	2.8 %	3.908 x 10^{-9}	7.0 %
3.162 x 10^{-5}	4.741 x 10^{-9}	3.5 %	3.669 x 10^{-9}	4.9 %
5.012 x 10^{-5}	4.513 x 10^{-9}	2.7 %	3.832 x 10^{-9}	3.8 %
7.943 x 10^{-5}	4.637 x 10^{-9}	3.0 %	3.767 x 10^{-9}	3.7 %
1.259 x 10^{-4}	4.565 x 10^{-9}	2.7 %	3.898 x 10^{-9}	3.8 %
1.995 x 10^{-4}	4.873 x 10^{-9}	3.3 %	3.845 x 10^{-9}	4.8 %
3.162 x 10^{-4}	4.947 x 10^{-9}	4.2 %	4.005 x 10^{-9}	3.4 %
5.012 x 10^{-4}	5.015 x 10^{-9}	2.8 %	4.204 x 10^{-9}	3.8 %
7.943 x 10^{-4}	5.385 x 10^{-9}	2.8 %	4.401 x 10^{-9}	4.6 %
1.259 x 10^{-3}	5.343 x 10^{-9}	3.1 %	5.439 x 10^{-9}	4.7 %
1.995 x 10^{-3}	5.686 x 10^{-9}	2.9 %	5.681 x 10^{-9}	4.5 %
3.162 x 10^{-3}	6.198 x 10^{-9}	4.6 %	6.172 x 10^{-9}	4.8 %
5.012 x 10^{-3}	7.151 x 10^{-9}	3.7 %	7.856 x 10^{-9}	4.5 %
7.943 x 10^{-3}	8.247 x 10^{-9}	3.8 %	1.111 x 10^{-8}	4.2 %
1.259 x 10^{-2}	1.111 x 10^{-8}	3.7 %	1.379 x 10^{-8}	3.8 %
1.995 x 10^{-2}	1.685 x 10^{-8}	3.7 %	1.926 x 10^{-8}	3.5 %
3.162 x 10^{-2}	2.525 x 10^{-8}	3.1 %	2.719 x 10^{-8}	3.1 %
5.012 x 10^{-2}	4.448 x 10^{-8}	2.6 %	4.168 x 10^{-8}	2.6 %
7.943 x 10^{-2}	8.244 x 10^{-8}	1.8 %	6.514 x 10^{-8}	2.1 %
1.259 x 10^{-1}	1.479 x 10^{-7}	1.4 %	1.045 x 10^{-7}	1.6 %
1.995 x 10^{-1}	2.747 x 10^{-7}	1.0 %	1.772 x 10^{-7}	1.3 %
3.162 x 10^{-1}	4.983 x 10^{-7}	0.8 %	2.790 x 10^{-7}	1.4 %
5.012 x 10^{-1}	8.735 x 10^{-7}	0.6 %	4.194 x 10^{-7}	0.8 %
7.943 x 10^{-1}	1.475 x 10^{-6}	0.4 %	5.923 x 10^{-7}	0.7 %
1.259 x 10^{0}	2.227 x 10^{-6}	0.3 %	7.211 x 10^{-7}	0.6 %
1.995 x 10^{0}	2.885 x 10^{-6}	0.3 %	1.007 x 10^{-6}	0.5 %
3.162 x 10^{0}	2.970 x 10^{-6}	0.3 %	2.160 x 10^{-6}	0.3 %
5.012 x 10^{0}	2.083 x 10^{-6}	0.4 %	3.851 x 10^{-6}	0.3 %
7.943 x 10^{0}	8.399 x 10^{-7}	0.6 %	3.946 x 10^{-6}	0.2 %
1.259 x 10^{1}	1.473 x 10^{-7}	1.4 %	1.117 x 10^{-6}	0.5 %
1.995 x 10^{1}	7.050 x 10^{-9}	6.3 %	0.0	0.0 %
3.162 x 10^{1}	5.625 x 10^{-11}	70.7 %	0.0	0.0 %
Total	1.4881 x 10^{-5}	0.03 %	1.4777 x 10^{-5}	0.04%

APPENDIX 4: Measured and calculated ^{252}Cf spectra at 150 cm from the source.

Energy	Total spectrum (free-field + scatter)			Scatter spectrum		
(MeV)	Measurement	MCNP	Ratio	Measurement	MCNP	Ratio
7.943×10^{-10}	6.438E-11	6.512E-11	0.989	6.197E-11	6.512E-11	0.952
1.259×10^{-9}	1.302E-10	1.322E-10	0.985	1.236E-10	1.322E-10	0.935
1.995×10^{-9}	4.929E-10	5.028E-10	0.980	4.602E-10	5.028E-10	0.915
3.162×10^{-9}	1.113E-09	1.141E-09	0.975	1.019E-09	1.141E-09	0.893
5.012×10^{-9}	2.688E-09	2.772E-09	0.970	2.407E-09	2.772E-09	0.868
7.943×10^{-9}	5.647E-09	5.860E-09	0.964	4.937E-09	5.860E-09	0.842
1.259×10^{-8}	1.315E-08	1.374E-08	0.957	1.116E-08	1.374E-08	0.812
1.995×10^{-8}	2.194E-08	2.309E-08	0.950	1.809E-08	2.309E-08	0.783
3.162×10^{-8}	3.250E-08	3.444E-08	0.944	2.601E-08	3.444E-08	0.755
5.012×10^{-8}	3.498E-08	3.720E-08	0.940	2.725E-08	3.720E-08	0.733
7.943×10^{-8}	2.471E-08	2.623E-08	0.942	1.935E-08	2.623E-08	0.738
1.259×10^{-7}	1.087E-08	1.148E-08	0.946	8.692E-09	1.148E-08	0.757
1.995×10^{-7}	4.814E-09	5.069E-09	0.950	3.907E-09	5.069E-09	0.771
3.162×10^{-7}	4.294E-09	4.512E-09	0.952	3.514E-09	4.512E-09	0.779
5.012×10^{-7}	3.916E-09	4.104E-09	0.954	3.237E-09	4.104E-09	0.789
7.943×10^{-7}	3.881E-09	4.058E-09	0.956	3.241E-09	4.058E-09	0.799
1.259×10^{-6}	4.198E-09	4.379E-09	0.959	3.538E-09	4.379E-09	0.808
1.995×10^{-6}	3.878E-09	4.035E-09	0.961	3.304E-09	4.035E-09	0.819
3.162×10^{-6}	4.464E-09	4.636E-09	0.963	3.830E-09	4.636E-09	0.826
5.012×10^{-6}	4.576E-09	4.743E-09	0.965	3.958E-09	4.743E-09	0.835
7.943×10^{-6}	4.160E-09	4.303E-09	0.967	3.630E-09	4.303E-09	0.844
1.259×10^{-5}	4.656E-09	4.809E-09	0.968	4.086E-09	4.809E-09	0.850
1.995×10^{-5}	4.372E-09	4.509E-09	0.970	3.869E-09	4.509E-09	0.858
3.162×10^{-5}	4.319E-09	4.447E-09	0.971	3.851E-09	4.447E-09	0.866
5.012×10^{-5}	4.483E-09	4.610E-09	0.972	4.028E-09	4.610E-09	0.874
7.943×10^{-5}	5.215E-09	5.357E-09	0.973	4.723E-09	5.357E-09	0.882
1.259×10^{-4}	4.830E-09	4.954E-09	0.975	4.424E-09	4.954E-09	0.893
1.995×10^{-4}	4.903E-09	5.021E-09	0.976	4.522E-09	4.999E-09	0.905
3.162×10^{-4}	5.027E-09	5.139E-09	0.978	4.701E-09	5.117E-09	0.919
5.012×10^{-4}	4.812E-09	4.909E-09	0.980	4.596E-09	4.909E-09	0.936
7.943×10^{-4}	5.229E-09	5.322E-09	0.983	5.091E-09	5.322E-09	0.957
1.259×10^{-3}	5.494E-09	5.573E-09	0.986	5.413E-09	5.506E-09	0.983
1.995×10^{-3}	5.417E-09	5.472E-09	0.990	5.496E-09	5.405E-09	1.017
3.162×10^{-3}	6.537E-09	6.568E-09	0.995	6.547E-09	6.188E-09	1.058
5.012×10^{-3}	6.518E-09	6.503E-09	1.002	6.595E-09	5.944E-09	1.110
7.943×10^{-3}	7.505E-09	7.424E-09	1.011	7.276E-09	6.214E-09	1.171
1.259×10^{-2}	9.781E-09	9.578E-09	1.021	9.021E-09	7.263E-09	1.242
1.995×10^{-2}	1.226E-08	1.187E-08	1.033	1.071E-08	8.104E-09	1.322
3.162×10^{-2}	1.801E-08	1.722E-08	1.046	1.232E-08	8.773E-09	1.405
5.012×10^{-2}	3.091E-08	2.918E-08	1.059	1.752E-08	1.175E-08	1.491
7.943×10^{-2}	5.024E-08	4.687E-08	1.072	2.374E-08	1.508E-08	1.574
1.259×10^{-1}	9.366E-08	8.640E-08	1.084	4.347E-08	2.606E-08	1.668
1.995×10^{-1}	1.594E-07	1.451E-07	1.099	5.453E-08	3.127E-08	1.744
3.162×10^{-1}	2.609E-07	2.341E-07	1.114	6.093E-08	3.409E-08	1.787
5.012×10^{-1}	4.501E-07	3.983E-07	1.130	1.073E-07	5.746E-08	1.868
7.943×10^{-1}	6.606E-07	5.858E-07	1.128	1.029E-07	5.699E-08	1.805
1.259×10^{0}	7.822E-07	7.441E-07	1.051	6.921E-08	5.051E-08	1.370
1.995×10^{0}	7.890E-07	7.670E-07	1.029	5.593E-08	4.319E-08	1.295
3.162×10^{0}	5.294E-07	5.228E-07	1.013	2.156E-08	1.736E-08	1.242
5.012×10^{0}	2.140E-07	2.118E-07	1.011	4.802E-09	3.985E-09	1.205
7.943×10^{0}	3.776E-08	3.738E-08	1.010	2.431E-10	2.088E-10	1.164
1.259×10^{1}	1.592E-09	1.584E-09	1.005	1.123E-33	1.000E-33	1.123
Total	4.366E-06	4.126E-06	1.058	8.211E-07	6.469E-07	1.269

FIGURE CAPTIONS

Figure 1. Section at x=970cm, showing the thermal pile and entrance to the labyrinth.

Figure 2. Section at x=1550cm: wall and roof of the Van de Graaff generator room.

Figure 3. Section at y=-0.5cm: the low-scatter facility and walls of the Van de Graaff generator room.

Figure 4. Low-scatter facility expanded to show the source-holding rod, the detector carriage tubes (centre and left) and one of the Aerolam walkways (right). The tally cells at 75cm and 150cm can also be seen.

Figure 5. Section at y=300cm. Includes the steel grid floor around the pit-circle and the thermal pile.

Figure 6. Section at z=487.1cm of the pit-circle: shows the three Aerolam walkways, detector carriage tubes and steel grid floor.

Figure 7. Section at z=590cm (source height). The maze at the entrance to the Main Bay and the walls of the Van de Graaff generator room can be seen. The two tallying cells at 75cm and 150cm around the source have also been drawn.

Figure 8. ^{252}Cf spectrum at two distances from the neutron source.

Figure 9. ^{241}Am-Be spectrum at two distances from the source.

Figure 10. In-scattered spectra at 75 cm and 150 cm from a ^{252}Cf source.

Figure 11. In-scattered spectra at 75 cm and 150 cm from a ^{241}Am-Be source.

Figure 12. Measured and calculated ^{252}Cf scatter spectrum in the NPL Main Bay.

Figure 13. MCNP model of the experimental set-up for measuring neutron scatter in the central region of the low-scatter facility.

Figure 14. Personal dosemeter response functions.

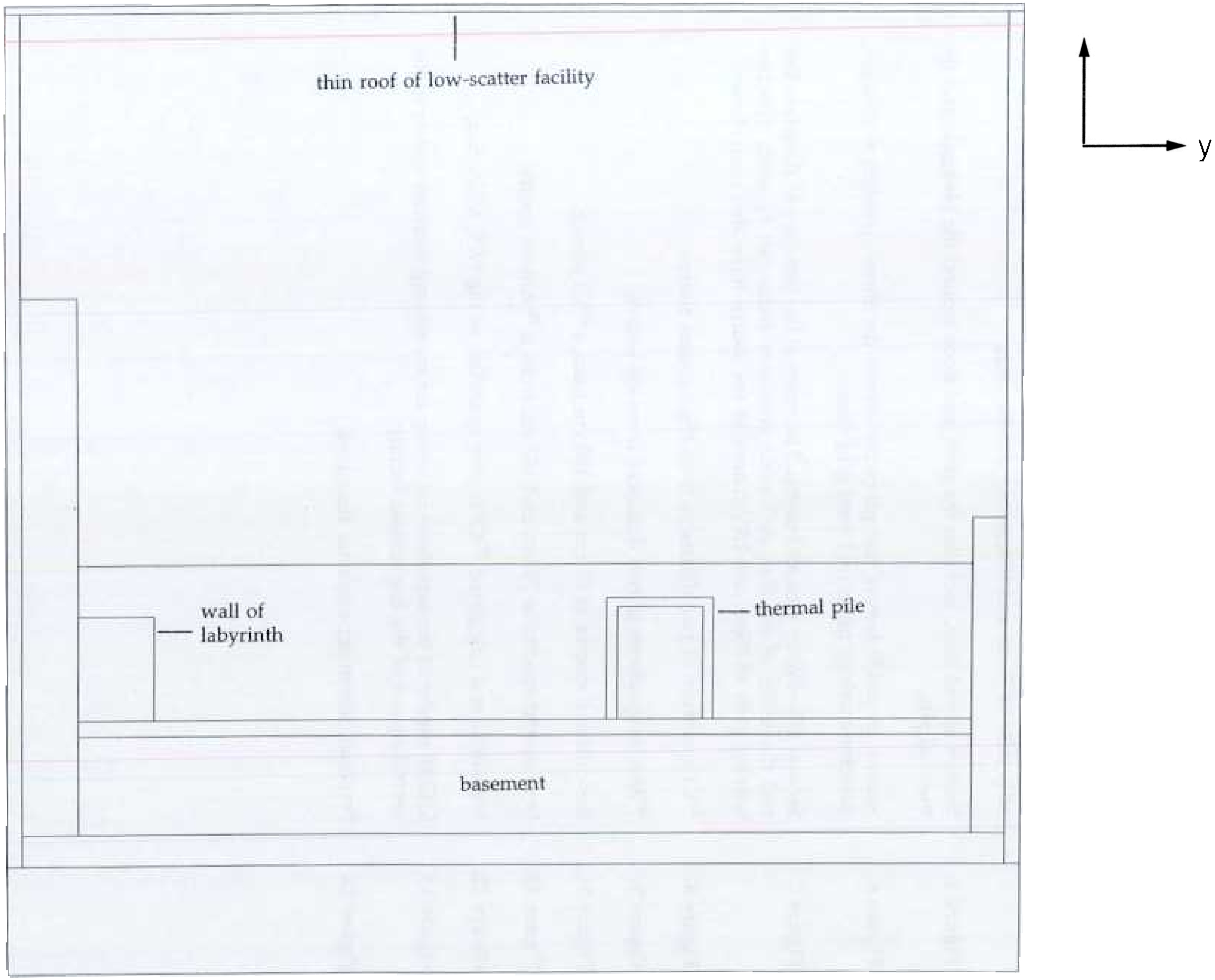

Figure Secti =970cm, showin the thermal pile and trance to the labyrinth.

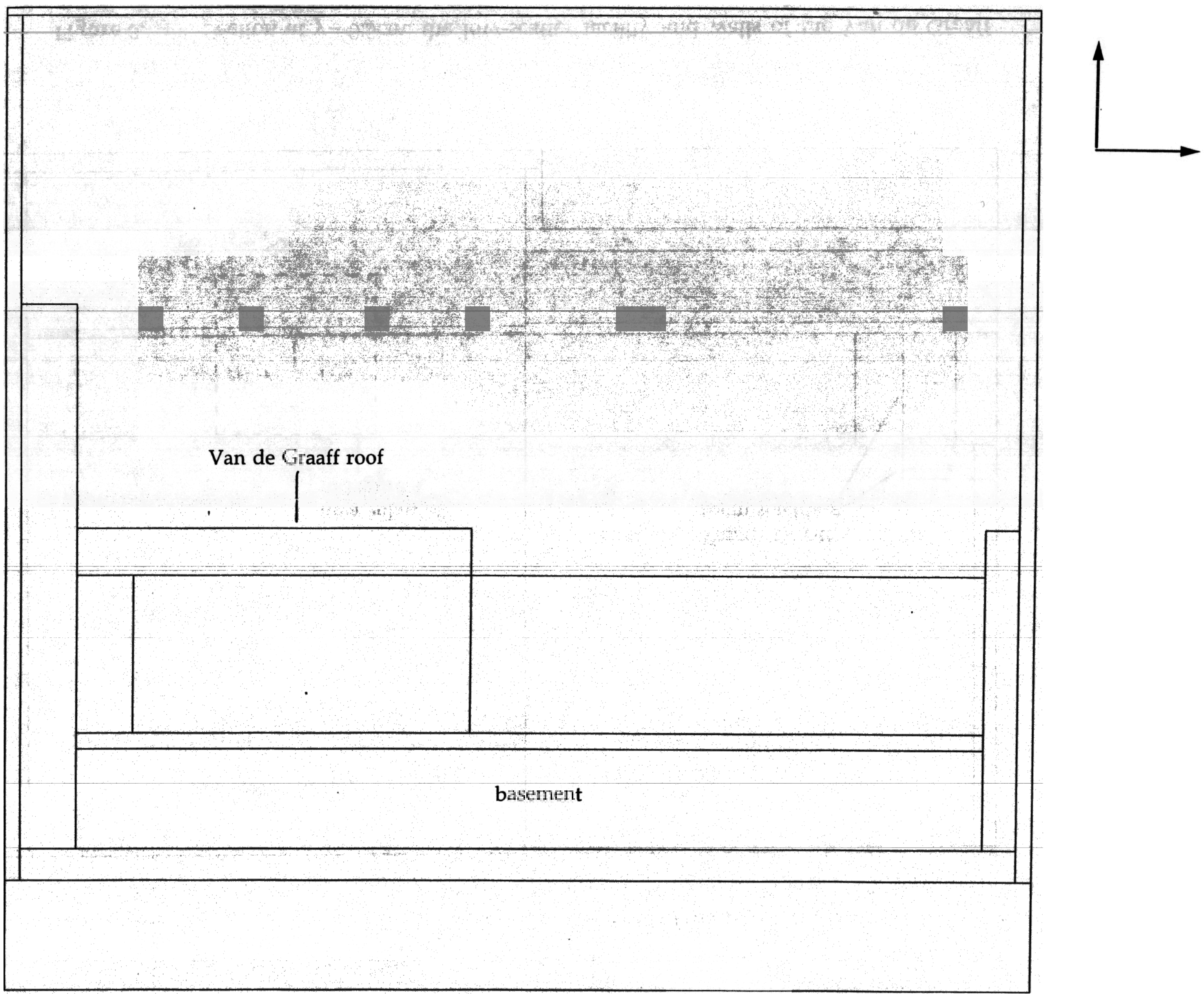

igure 2. Sectio 550cm 'all and roof the V G aff generator room.

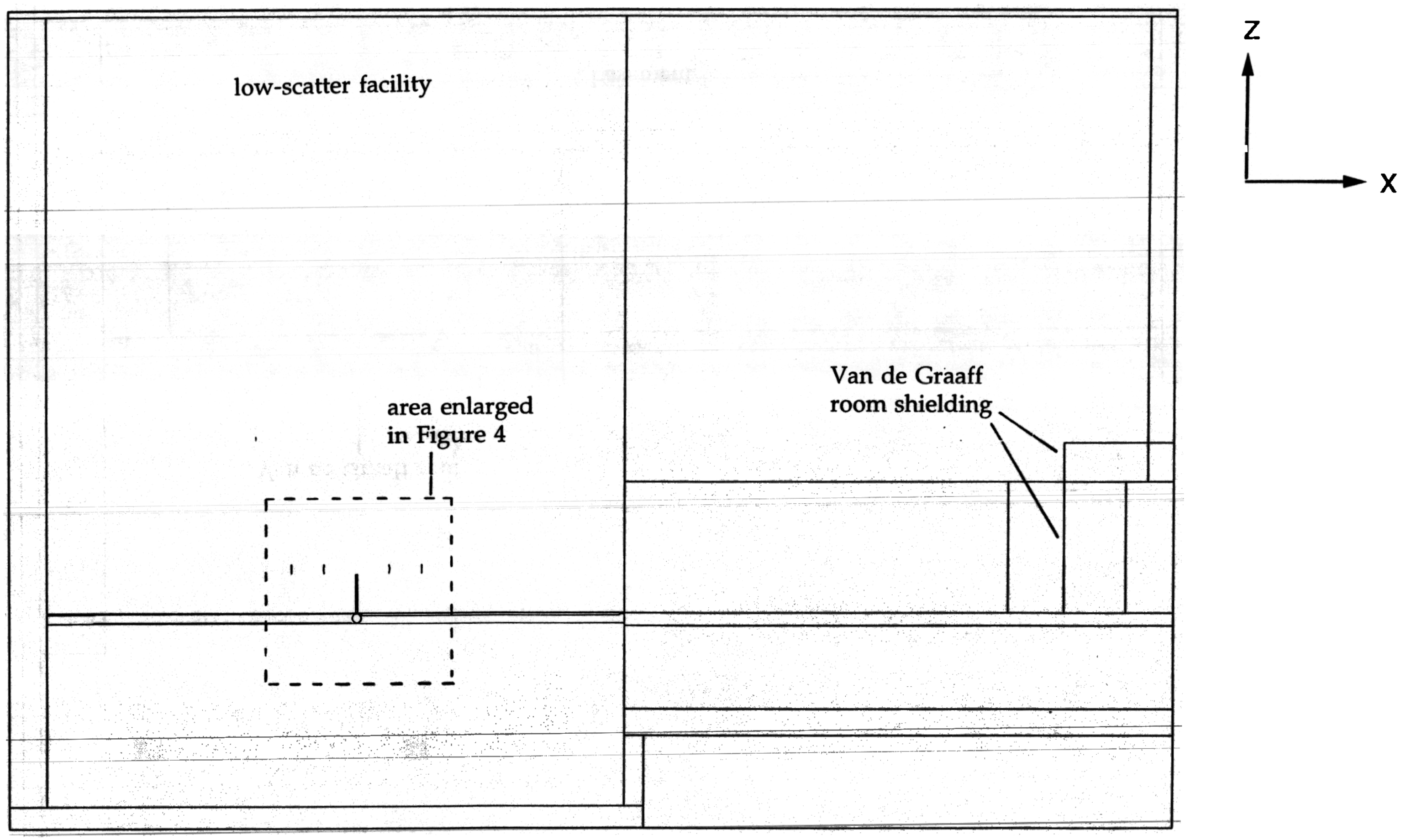

Figure 3. Section at y=-0.5cm: the low-scatter facility and walls of the Van de Graaff generator room.

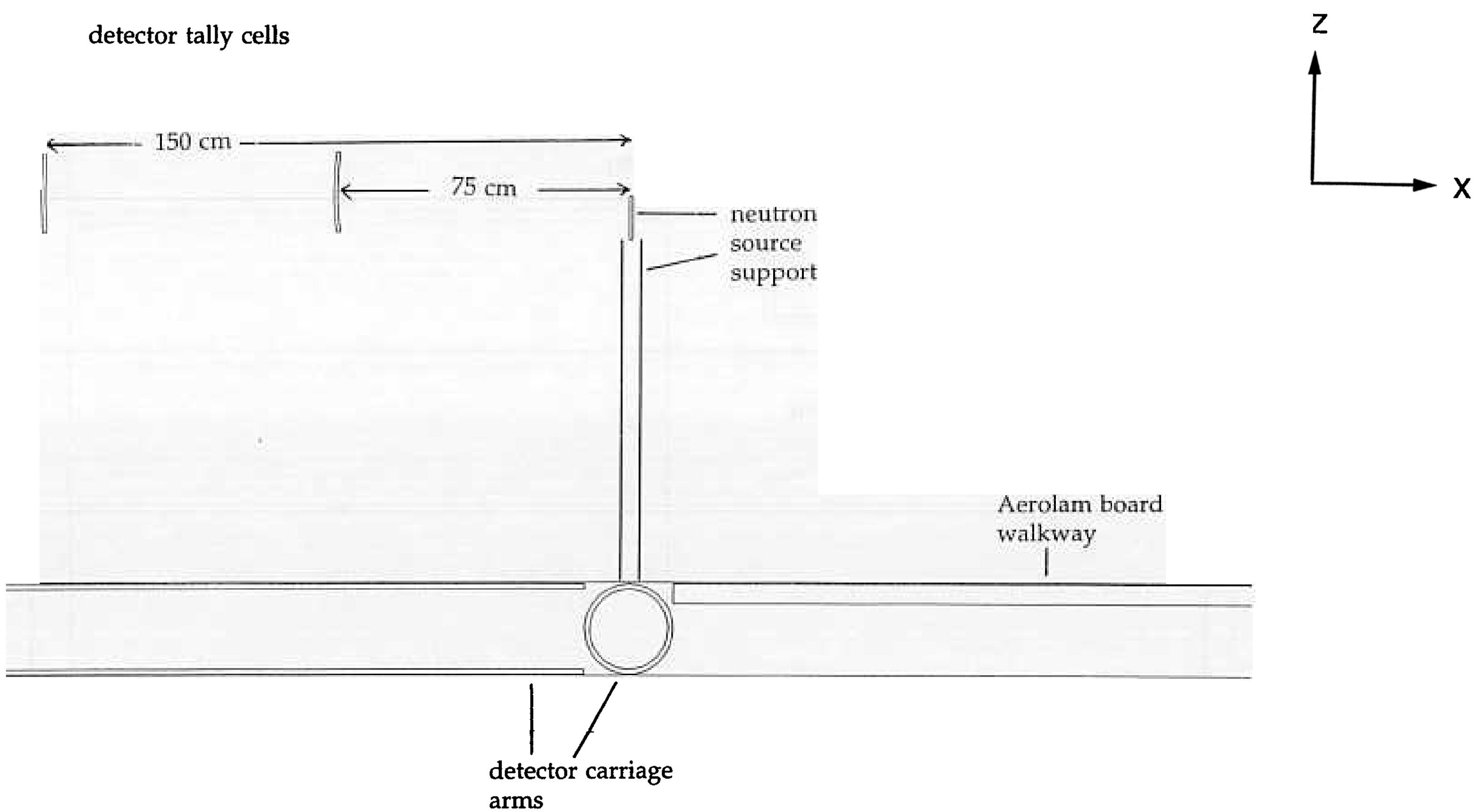

Figure 4. Low-scatter facility expanded to show the source-holding rod, the detector carriage tubes (centre and left) and one of the Aerolam walkways (right). The tally cells at 75cm and 150cm can also be seen.

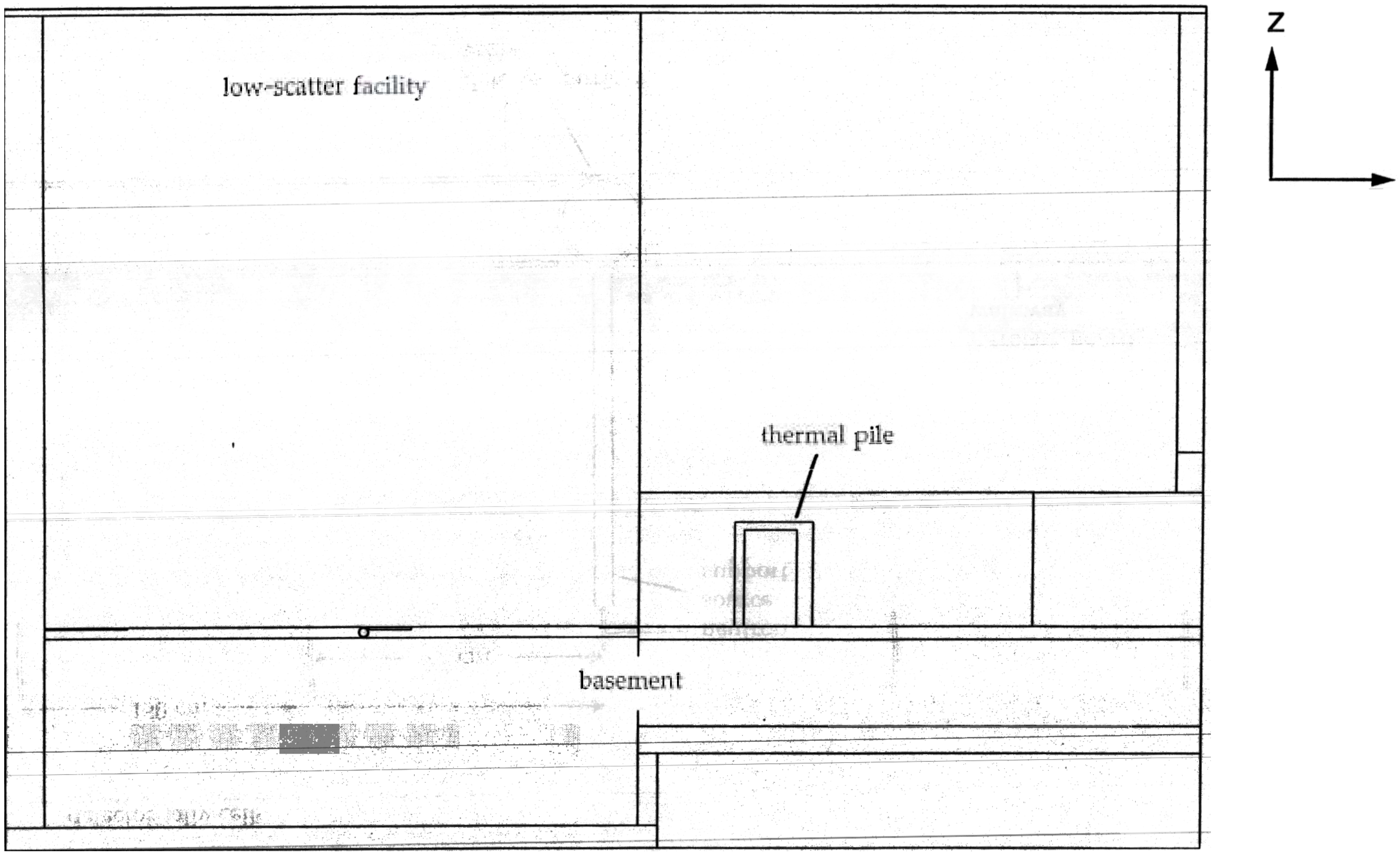

Figure 5. Section at y=300cm. Includes the steel grid floor around the pit-circle and the thermal pile

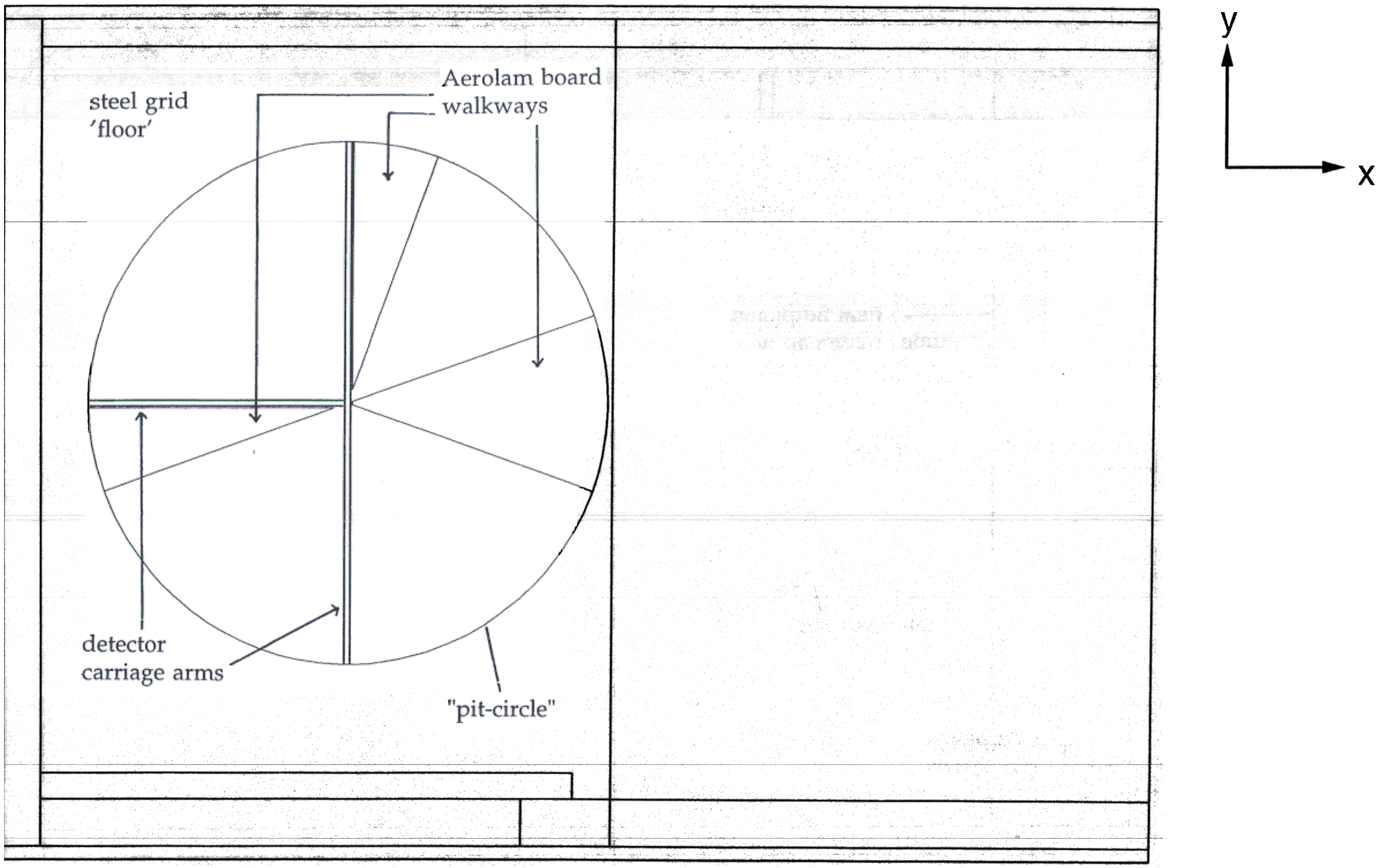

Figure 6. Section at z=487.1cm of the pit-circle: shows the three Aerolam walkways, detector carriage tubes and steel grid floor.

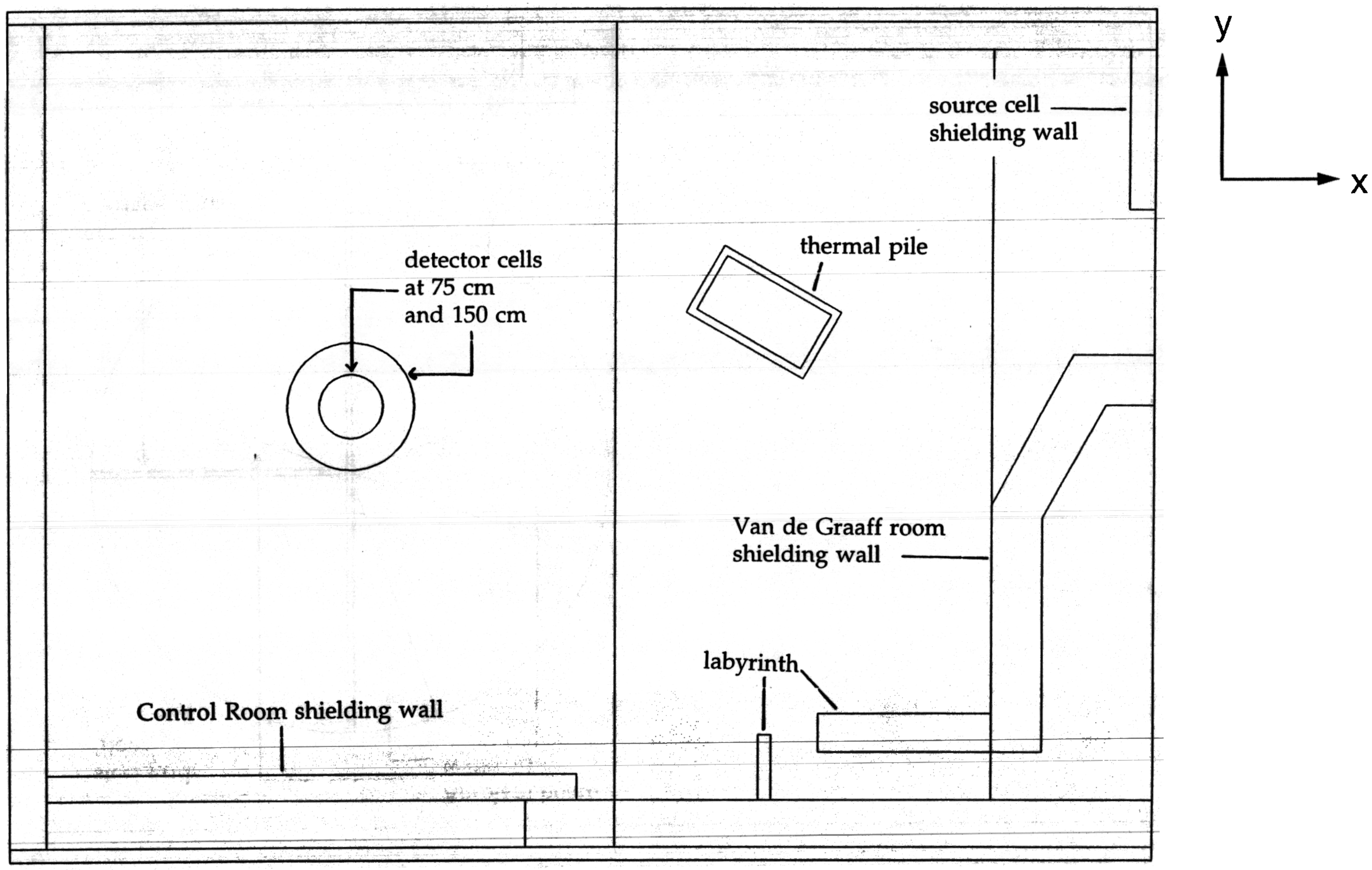

Figure 7. Section at z=590cm (source height). The maze at the entrance to the Main Bay and the walls of the Van de Graaff generator room can be seen. The two tallying cells at 75cm and 150cm around the source have also been drawn.

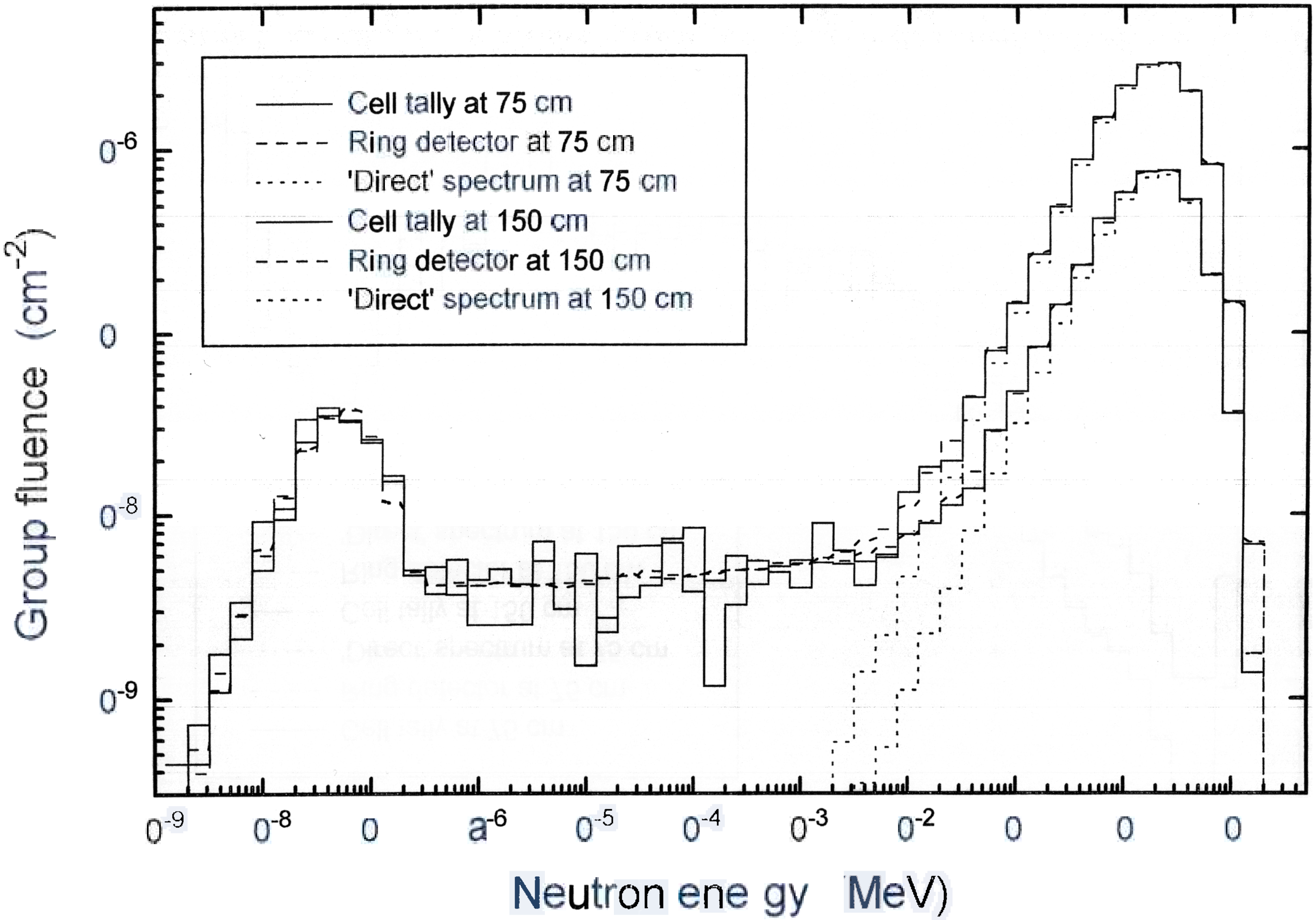

Figure ^{252}Cf spectrum tw distances from the neutron

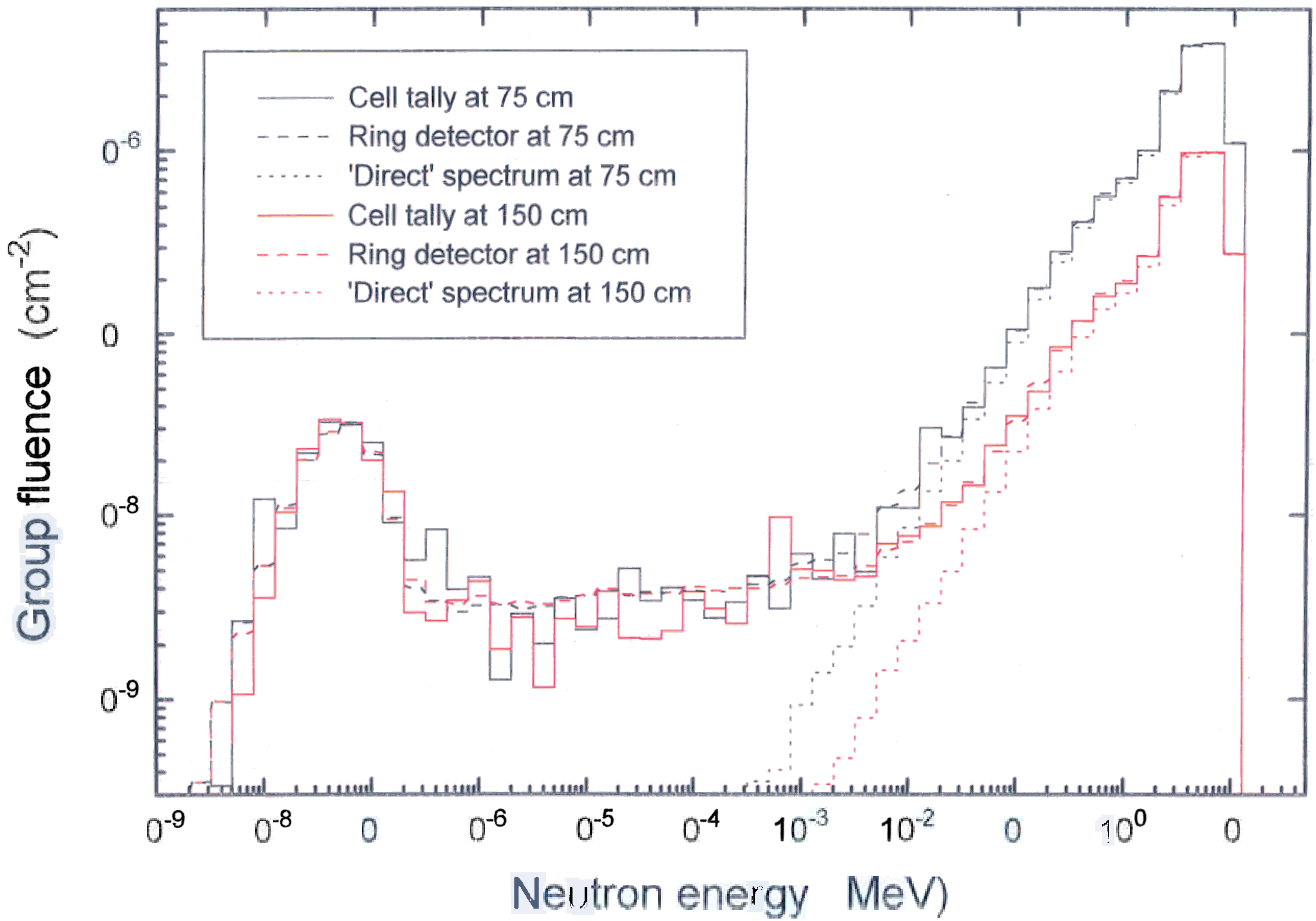

Figure ^{241}Am-Be pectrum tw distances from the source

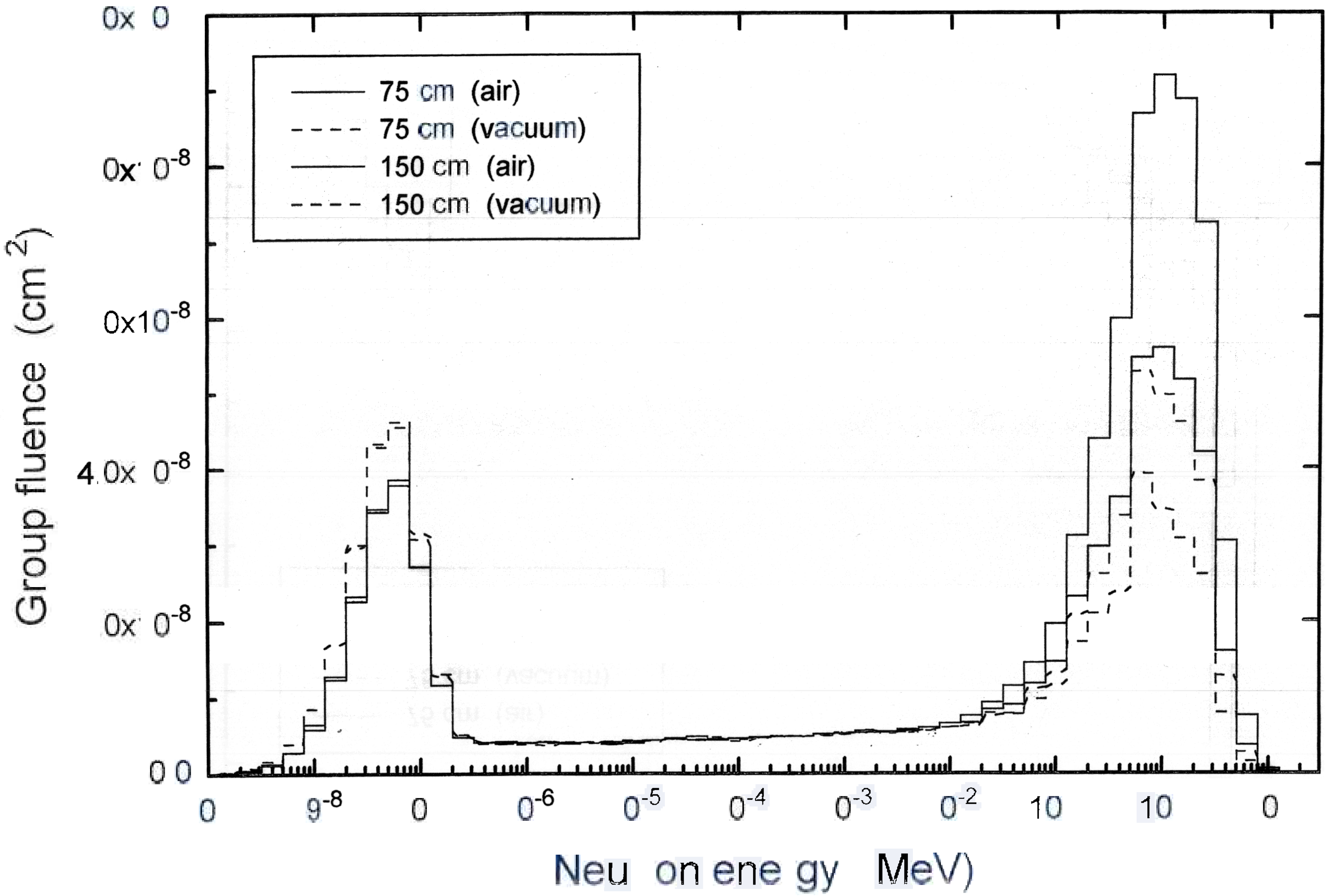

Figure In-sc tte spec 50 fr ^{252}Cf so

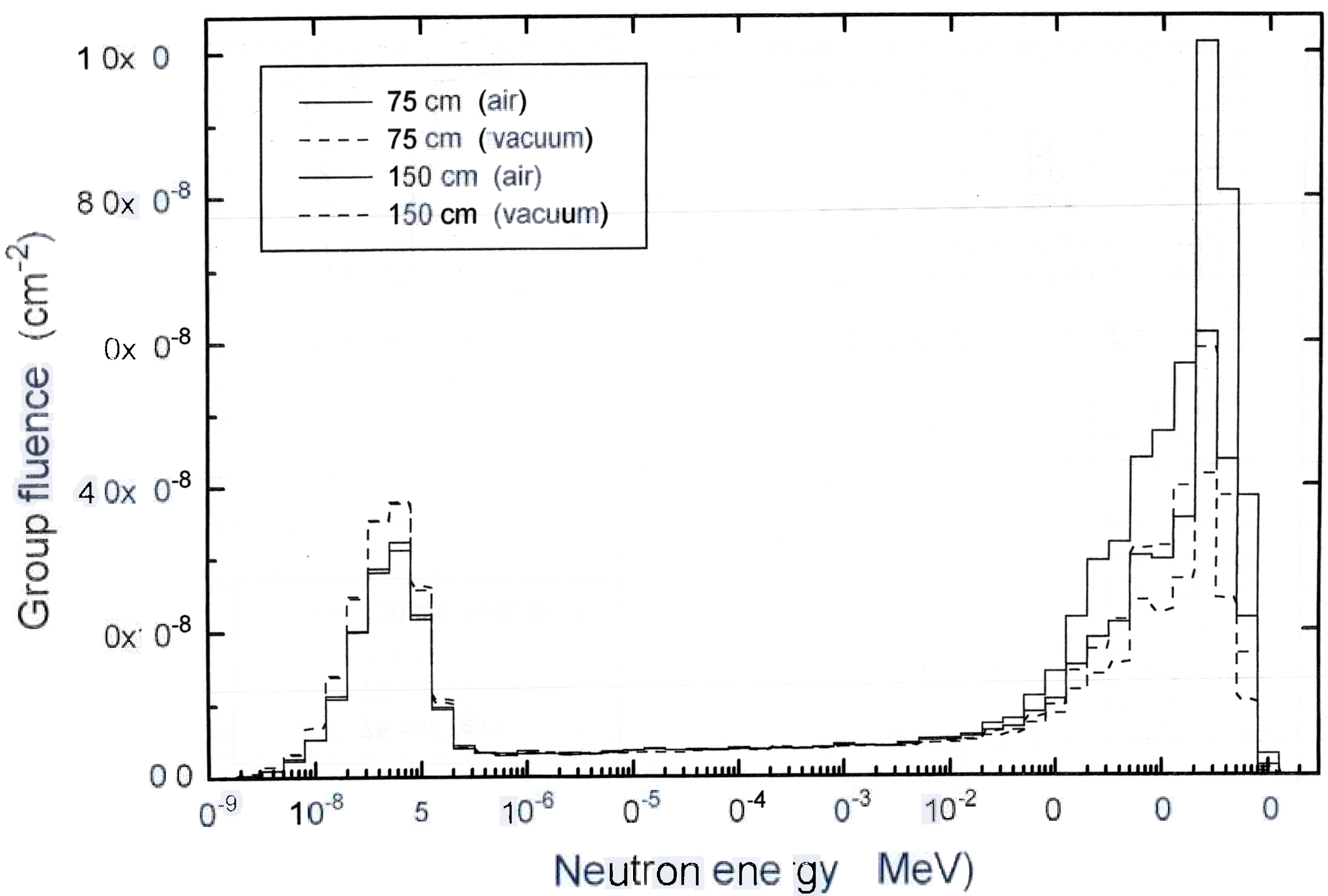

Figure In tered spectr 75 and 50 from Am-Be source

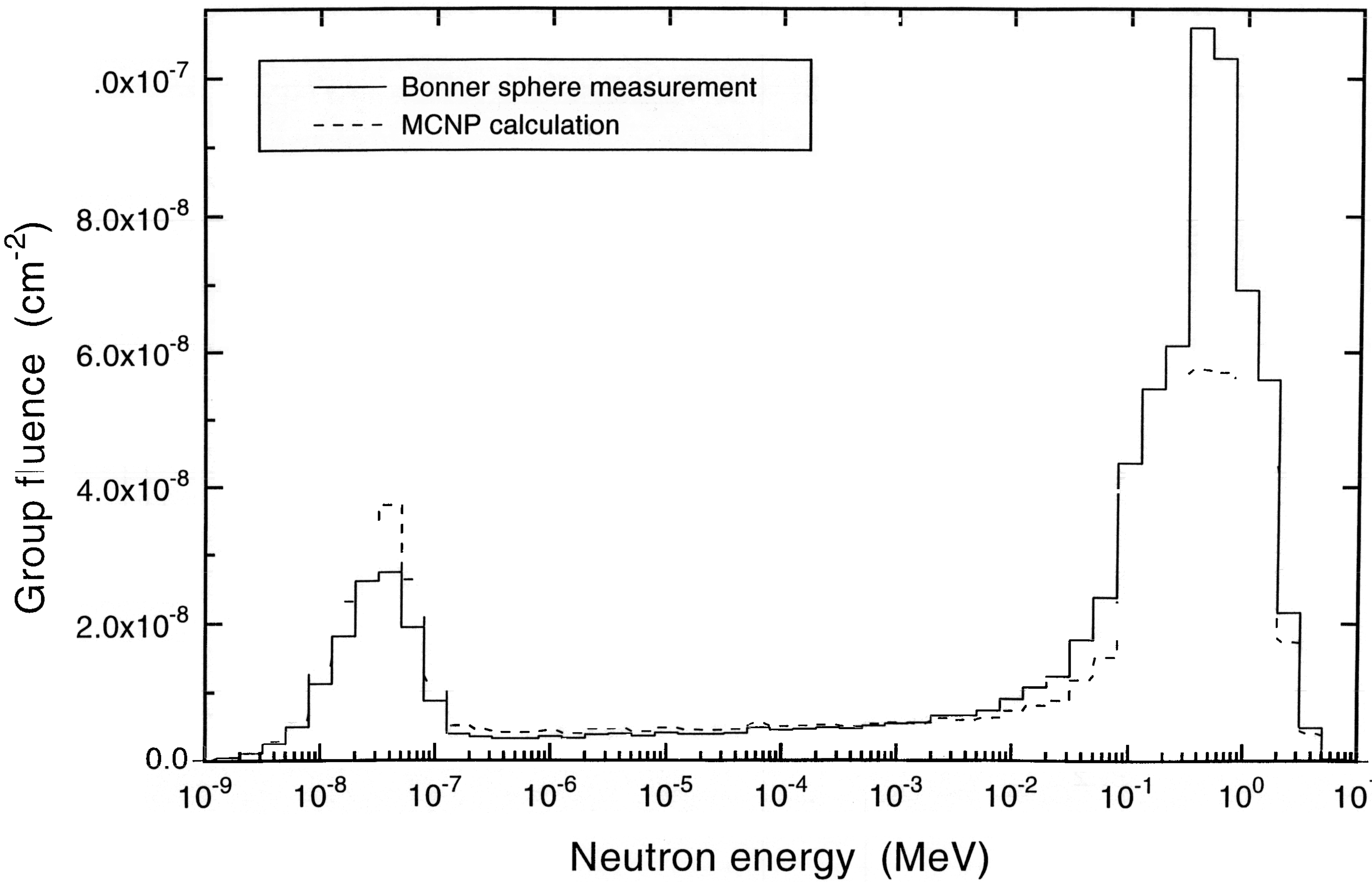

Figure 12. Measured and calculated ^{252}Cf scatter spectrum in the NPL Main Bay.

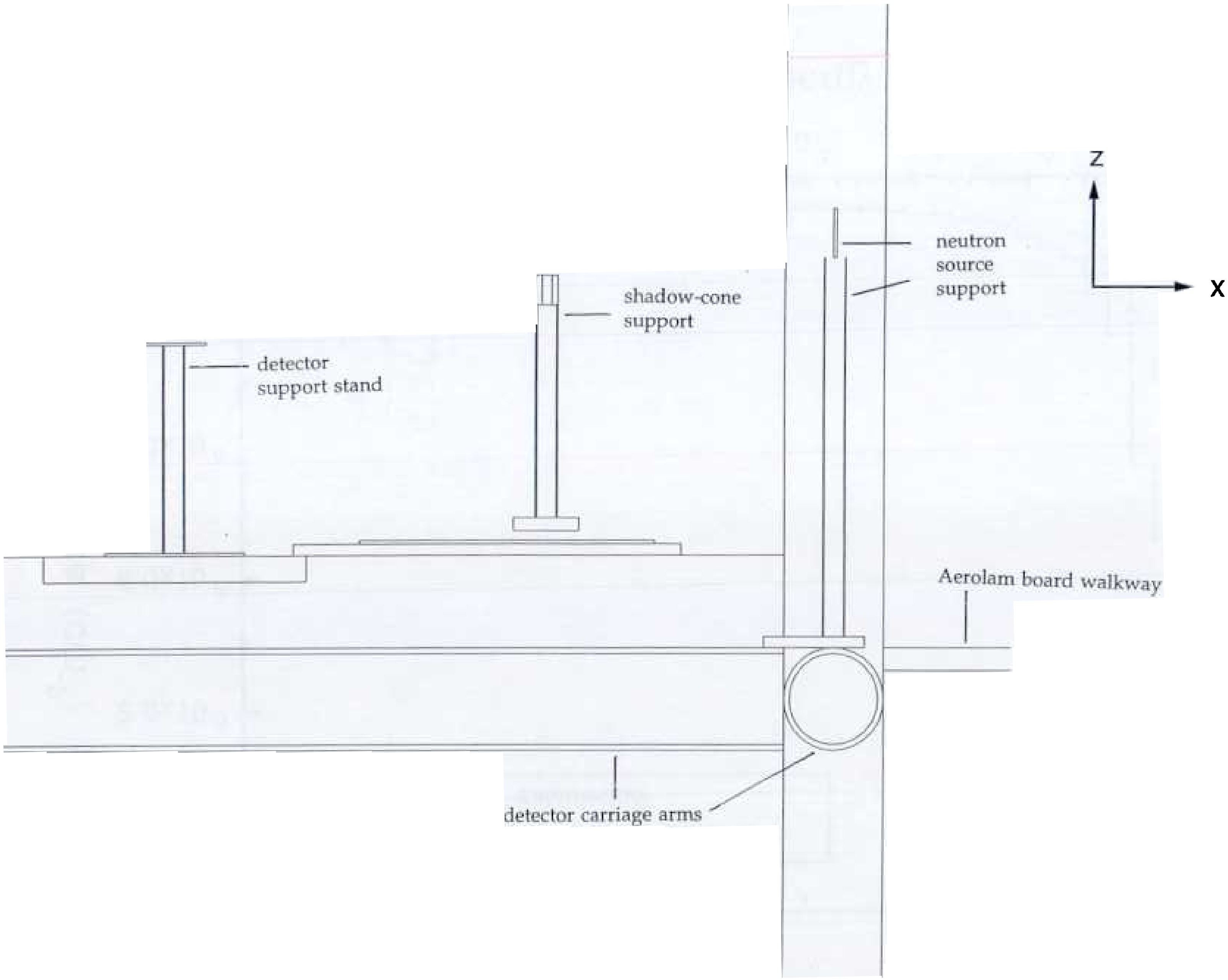

Figure 13. MCNP model of the experimental set-up for measuring neutron scatter in the central region of the low-scatter facility.

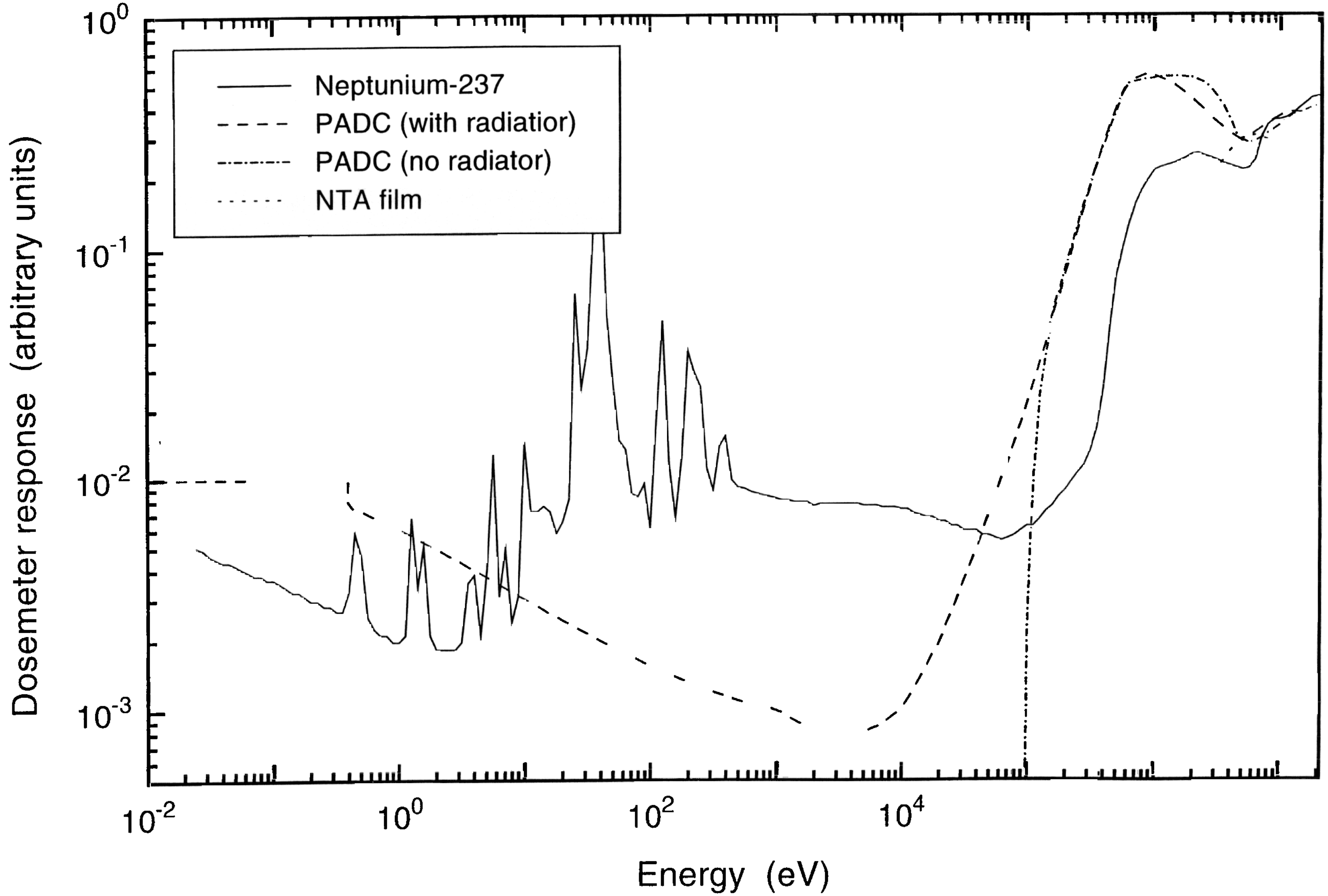

Figure 14. Personal dosemeter response functions.